SURFACE WAVE DISPRESION BETWEEN NORTH AND EAST AFRICA

by

FEKADU KEBEDE

A Thesis

Submitted to the

School of Graduate Studies

and

the Faculty of Science in the

Addis Ababa University

In Partial Fulfillment

of the Requirements for the Degree

Master of Science in Physics

June 1983

D E C L A R A T I O N

I, the undersigned, declare that this thesis has been submitted for examination with my approval as a university advisor.

Name Dr. Laike Mariam Asfaw

Signature

ACKNOWLEDGMENTS

I wish to express my personal gratitude to my advisor, Dr. Laike M. Asfaw (AAU) for his frequent advice, stimulating discussions, valuable critisms and help in organizing the paper.

I am highly grateful to Ato Ghebrebrhan Ogubazghi (AAU) for his helpful suggestions and disscussions; Dr. Waverly J. Person (United States Department of Interior Geological Survey) and Dr. Robert H. Herrman (Saint Louis University) for providing computer programs; Dr. A. Douglas (International Seismological Center) for providing tables for correction group time delay due to instrumental response.

My acknowledgements also go to the following staff members of the Geophysical Observatory (AAU). W/t Almaz Armide and W/t Manyahilishal Sebsibe, for typing; Ato Alemu Mamo and Ato Yirga Tesfaye for drafting works.

My thank is also due to Dr. Shibru Tedla (AAU) for his cooperation in making available an article in time.

Finally, Special thank is due to Geophysical Observatory (AAU) for providing the data and other facilities.

CONTENTS

ILLUSTRATIONS

List of figures

List of tables

ABSTRACT

A comprehensive study of dispersion of surface Rayleigh waves for three paths: Gulf of Aden - Addis Ababa (GOA - AAE), Red Sea Addis Ababa (RES - AAE) and Arab republic of Egypt - Addis Ababa (ARE - AAE), lying between north and east Africa is made. Earlier studies of surface wave dispersion in the region were made for short epicentral distances without considering contribution by different modes. The problem of contribution by different modes to dispersion is inherent at short epicentral distance ranges.

Rayleigh wave trains identified from seismograms of Addis Ababa seismic station (AAE) are enlarged and digitized. The results are analysed using fixed window Fourier analysis and moving window analysis (Landisman et al. 1969). These methods have advantages in displaying different modes which otherwise would be absent if the usual peak and trough method is used.

Dispersion curves obtained by the above methods and the usual peak and trough method are compared with theoretical dispersion curves generated for different crustal models. An efficient algorithm developed for solving the period equation on a computer (Dunkin 1965; Robert H. Herrman personal communication 1980) is used to obtain theoretical dispersion curves up to ten modes. However, in this study the fundamental and first modes were found adequate to explain the seismogram observations. A total of 150 theoretical models each with multimode outputs were considered.

A crustal thickness of 27 km with high Poisson's ratio overlying an anomalous mantle (α = 7.2 km/sec) 4 km thick is found for GOA - AAE path. For RES - AAE and ARE - AAE paths crustal thicknesses of 37 km and 38 km respectively overlying a normal mantle are found. The Poisson's ratios for these paths are similar to that of a normal continental crust.

Regarding resolution of modes for the period range considered in this study both moving and fixed window methods give similar results indicating that the former method is superfluous.

CHAPTER I

INTRODUCTION

One method of studying the deep structure and properties of the earth which are not accessible to direct observation is the method of surface wave dispersion. This method utilizes records of elastic surface waves (from seismograms) generated by an earthquake or explosion which have travelled through the earth as the raw data to which a theoretical model that will best fit the data will be sought.

When applying the method of surface wave dispersion to study the internal structure and properties of the earth, the earth which has a free surface and numerous internal zones of contrasting physical properties is conceived to be represented by a number of physically distinct layers each with its own characteristic density, thickness and velocities of compressional and shear waves.

In the mathematical formulation of the problem the physical properties of the layers cited above will determine the dispersion relation, i.e., they will enter the period equation determining the type of relations between the period and velocity.

Subsequently we will study surface wave dispersion from North and North - East Africa for paths indicated in Figure 1 with a view to characterizing the physical properties of the crust by comparing dispersion curves obtained from records of earthquake surface waves with theoretically generated dispersion curves.

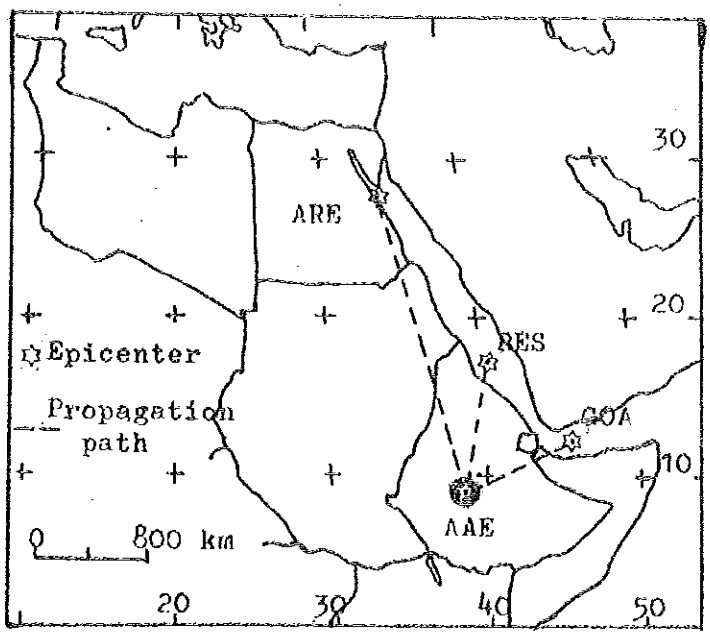

Fig. 1 Location of epicenters GOA, RES, ARE and seismograph station (AAE).

Table 1 gives region of each epicenter and names of paths to be adopted for future use.

Table 1 Region of epicenter and names of paths.

Recording Station	Epicenter location	Path as referred to in this study
AAE	Western Gulf of Aden	GOA - AAE
AAE	Red Sea	RES - AAE
AAE	Arab Rep. of Egypt	ARE - AAE

In the following we will recapitulate the relevant results obtained by earlier workers to set our task in perispective.

a) GOA - AAE path

This path is mainly a continental path except for few tens kilometers traversing the western Gulf of Aden. Jones (1968) and Searle (1975) made preliminary studies on dispersion of surface waves across the southern part of the Afar Depression. Their paths were slightly to the north of the path considered for this study. In his study Searle (1975) found a group velocity of Rayleigh waves as high as 3.5 km/sec and suggested that no unique model was superior to others to be accepted as a representative model for the path. However, no attempt was made to indicate contributions by higher modes which can't be avoided for such short epicentral distances. For example, Tryggvason (1962) has studied the crustal structure of the Iceland region for the same order of epicentral distance and identified the Rayleigh wave train to be a first mode Rayleigh wave. Therefore the high group velocity Searle (1975) obtained may be due to higher mode Rayleigh waves which he didn't consider.

This study will be made by considering the possiblity of modal contribution. For this purpose data from digitized seismograms (the method of analysis will be briefly discussed in chapter IV) are Fourier analysed and the contribution by various modes will be indicated.

For the path selected (GOA - AAE) the presence of an anomalous mantle as also shown by Gravity (Makris et al. 1972) and seismic sounding (Berckhemer et al. 1975) is verified and an

average thickness of the anomalous mantle for the path is found. In this respect the present study extends the work done on dispersion for this path in particular.

b) RES - AAE path

This path is also largely a continental path. The epicenter lies in the continental shelf of the Red Sea. For this path no work has been done on dispersion up to the present.

From a preliminary study of travel times of near earthquakes Searle and Gouin (1971) suggested an upper limit for the thickness of the crust below the Ethiopian plateau to be about 48 km. Based on other geophysical methods, such as Gravity and Seismic sounding a mean crustal thickness of the Western Ethiopia plateau has been found to be 38 km.

Therefore, the purpose of this study regarding this path is to contribute towards a resolution of the ambiguity in the results obtained earlier.

c) ARE - AAE path

This path is totaly a continental path. Eventhough no detailed work by any geophysical method was made for this particular path, a general idea about the crustal structure can be inferred from a preliminary result of Sandos (Ph.D. thesis, not yet published, personal communication). Sandos found a mean crustal thickness for a path between HLW (Helwan recording station) and AAE to range from 35 - 40 km. However, Sandos

didn't consider contribution by different modes and give only a preliminary crustal structure using a single-layer model.

This paper improves the work of Sandos by considering modal contribution and approximating the crust by a three-layer crustal model.

As we have indicated at the outset, our main concern will be the study of surface wave dispersion. In the subsequent chapters we will develop the theoretical basis of this method and use it to model the crustal structure along the paths mentioned.

CHAPTER II

ELASTICITY THEORY AND ELASTIC SURFACE WAVES

2.1 Elasticity Theory

It is mentioned in chapter I that useful information on the earth's crust and the upper mantle can be found from elastic waves propagating in the earth. The velocity of propagation of elastic waves depends upon the elastic properties and densities of the materials through which they propagate. Elastic waves propagate in materials as patterns of particle deformation travelling in the materials. The elastic properties and densities of a medium are related through an expression for the velocity.

To show this dependence of elastic wave velocities upon elastic properties and densities we will briefly summarize the fundamentals of elasticity theory (Achenbach 1975, Sokolnikoff 1956) leading to elastic surface waves.

2.1.1 Notation

In the following tensor notation with all its properties will be used. Whenever there is deviation from the rule, especially summation, the usage will be indicated in a bracket.

The following are the notations used.

Symbol	Description
$\vec{X}$	Position vector with components x_i
$\vec{U}$	Displacement vector with components u_i
τ	Stress tensor with components $\tau_{x_i x_j} = \tau_{ij}$
e	Strain tensor with components $e_{x_i x_j} = e_{ij}$
$u_{i,j}$	$\partial u_i / \partial x_j$
$u_{i,ij}$	$\partial / \partial x_j \quad (\partial u_i / \partial x_i)$
$u_{i,t}$	$\partial u_i / \partial t = \dot{u}_i$

2.1.2 Strain

To analyse the state of deformation of a medium we will consider the deformation in a neighbourhood of a particle. Let the position of a particle and a neighbouring one before deformation be $\vec{X}$ and $\vec{X} + \delta\vec{X}$ respectively. After deformation the positions will be $\vec{X} + \vec{U}(\vec{X})$ and $\vec{X} + \delta\vec{X} + \vec{U}(\vec{X} + \delta\vec{X})$ for the particle initially at $\vec{X}$ and $\vec{X} + \delta\vec{X}$ respectively. Consideration of the difference between the two vectors joining the two points before and after deformation enables us to study the character of deformation in the neighbourhood of a particle. The new vector line-element is

$$\vec{X} + \delta\vec{X} + \vec{U}(\vec{X} + \delta\vec{X}) - (\vec{X} + \vec{U}(\vec{X})) = \delta\vec{X} + \vec{U}(\vec{X} + \delta\vec{X}) - \vec{U}(\vec{X}). \quad (2.1)$$

For small $|\delta\vec{X}|$, expanding $\vec{U}(\vec{X} + \delta\vec{X})$ in Taylor series and retaining terms up to the first order only we obtain

$$\vec{U}(\vec{X}+\delta\vec{X}) = \vec{U}(\vec{X}) + (\delta\vec{X}.\vec{\nabla})\vec{U}$$

or $$\delta\vec{U} = \vec{U}(\vec{X}+\delta\vec{X}) - \vec{U}(\vec{X}) = (\delta\vec{X}.\vec{\nabla})\vec{U} \tag{2.2}$$

In component form we can write this as

$$\delta u_i = \frac{\partial u_i}{\partial x_j}\,\delta x_j = u_{i,j}\,\delta x_j \,. \tag{2.3}$$

It is possible to decompose eq. (2.3) into pure deformation and rigid body motion by rewriting as

$$\delta u_i = \left(\left(\frac{u_{i,j} + u_{j,i}}{2}\right) + \left(\frac{u_{i,j} - u_{j,i}}{2}\right)\right)\delta x_j \tag{2.4}$$

or $$\delta u_i = (e_{ij} + w_{ij})\delta x_j \,. \tag{2.5}$$

Where $$e_{ij} = \tfrac{1}{2}(u_{i,j} + u_{j,i}) \tag{2.6}$$

and $$w_{ij} = \tfrac{1}{2}(u_{i,j} - u_{j,i}) \tag{2.7}$$

are called the strain and rotation tensors respectively.

When i = j (summation not implied) eq. (2.6) gives the relative changes in dimension along the x_i direction. These relative changes are called normal strains. When $i \neq j$ eq. (2.6) gives the change in shape of the body. These changes in shape of the body are called shearing strains. Eq. (2.7) gives a rotation of the medium about an axis. Therefore, it is not related to strain.

Let the volume of the body before and after deformation be

$$V_i = dx_1\, dx_2\, dx_3 \tag{2.8}$$

and $$V_f = dx_1(1+e_{11})\, dx_2(1+e_{22})\, dx_3(1+e_{33}) \tag{2.9}$$

respectively. Retaining the first order terms only the relative change in volume, designated by Θ and known as dilatation, can be shown to be

$$\Theta = \frac{\Delta V}{V_i} = e_{ii} \,. \tag{2.10}$$

2.1.3 Stress

If one wants to analyse the forces acting on a volume element ΔV inside a body, it is necessary to take into consideration the effect of two types of forces, namely, body forces and surface forces. Body forces are forces which are proportional to the material (mass) contained in the volume element under consideration. The second type of forces act on the surface ΔS of the volume element.

To get some idea about the components of stress, let us consider the surface forces by isolating an infinitesimal parallelepiped inside a stressed body.

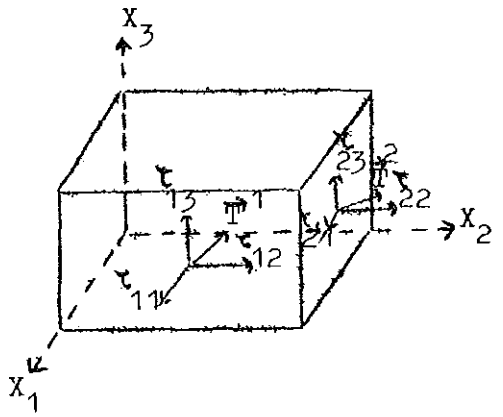

Fig. 2.1 Some of the stress components acting on a stressed body.

If the stress is not normal to the surface, it can be decomposed into its normal and tangential components called normal and shearing stresses respectively. Figure 2.1 shows some of the stress components acting on a stressed body. For example in the figure τ_{12} means a stress parallel to the X_2 axis acting upon a surface perpendicular to the X_1 axis (shearing stress). According to the convention, τ_{ii} (no summation) gives the normal stress in the X_i direction.

If $\vec{T}(\vec{X})$ denotes the distribution of stress vector acting on the surface S of a body, then by isolating a tetrahedron it can be shown that the components T_l of the stress vector can be expressed as

$$T_l = \tau_{kl} n_k \, . \tag{2.11}$$

Where τ_{kl} is the component of the stress in the X_l direction and n_k is the component of the normal to the surface.

The condition of equilibrium (vanishing of resultant force) of the body under surface and body forces can be expressed as

$$\int_v f_l \, dv + \int_s T_l \, ds = 0 \, . \tag{2.12}$$

Where f_l is the component of body force per unit volume. Using eq. (2.11) and Gauss' theorem it is possible to write eq. (2.12) as

$$\int_v f_l \, dv + \int_v \tau_{kl,k} \, dv = 0 \tag{2.13}$$

or

$$\int_v (f_l + \tau_{kl,k}) \, dv = 0. \tag{2.14}$$

Noting that the volume can be arbitrary eq. (2.14) yields

$$\tau_{kl,k} = -f_l . \tag{2.15}$$

Now, let us see the consequence of the vanishing of the resultant moment produced by body and surface forces. The resultant moment of the body force per unit volume can be written as the integral over the volume V of the vector product of the position vector $\vec{r}$ and the body force vector $\vec{f}$. This can be written componentwise as

$$M_i = \int_v \varepsilon_{ijk} x_j f_k \, dv . \tag{2.16}$$

Where ε_{ijk} is an alternating tensor. It is also possible to write similar expressions for the resultant moment of the surface forces in the form

$$B_i = \int_s \varepsilon_{ijk} x_j \tau_{lk} n_l ds. \tag{2.17}$$

Thus, the total resultant moment for equilibrium case can be written as

$$R_i = \int_v \varepsilon_{ijk} x_j f_k dv + \int_v (\varepsilon_{ijk} x_j \tau_{lk}),_l dv = 0 . \tag{2.18}$$

But $\int_v (\varepsilon_{ijk} x_j \tau_{lk}),_l dv = \int_v \varepsilon_{ijk}(x_j \tau_{lk,l} + \delta_{jl} \tau_{lk}) dv.$

. . . . (2.19)

Where δ_{jl} is the Kronecker delta symbol and

$$\delta_{jl} \tau_{lk} = \tau_{jk} . \tag{2.20}$$

Using eq. (2.15) eq. (2.19) gives

$$\int_v \varepsilon_{ijk}(x_j \tau_{lk,l} + \delta_{jl} \tau_{lk}) dv = \int_v \varepsilon_{ijk}(-x_j f_k + \tau_{jk}) dv. \tag{2.21}$$

Substitution of eq. (2.21) into eq. (2.18) readily gives

$$\int_v \varepsilon_{ijk} \tau_{jk} dv = 0 . \tag{2.22}$$

Since the volume can be arbitrary eq. (2.22) yields

$$\varrho_{ijk}\,\tau_{jk} = 0 \qquad (2.23)$$

and this implies

$$\tau_{jk} = \tau_{kj} \,. \qquad (2.24)$$

2.1.4 Stress - Strain relation for a homogenous, isotropic, elastic solid and elastic constants.

We have already established in the previous sections that the state of stress is completely determined by the stress tensor τ_{ij} and the state of deformation by the strain tensor ϱ_{ij}. In this section we will briefly show the relationship between stress and strain. In general, for a linearly elastic material the relationship between the stress and strain can be written as

$$\tau_{ij} = \varsigma_{ijkl}\,\varrho_{kl}. \quad i,j,k,l = 1,2,3 \,. \qquad (2.25)$$

Where ς_{ijkl} are elastic constants of the medium.

In general the coefficients ς_{ijkl} vary from point to point in the medium. If the coefficients ς_{ijkl} are not dependent on the position of a point in a medium, the medium is called a homogenous medium.

We have already shown that the stress components τ_{ij} are symmetric. This symmetry of the stress components allows us to write the coefficients ς_{ijkl} as

$$\varsigma_{ijkl} = \varsigma_{jikl}. \qquad (2.26)$$

One can easily see from eq. (2.6) that

$$e_{kl} = e_{lk} . \tag{2.27}$$

This symmetry condition implies

$$c_{ijkl} = c_{ijlk} . \tag{2.28}$$

From the above conditions of symmetry of c_{ijkl} we can only have at most 36 independent elastic constants in the general stress-strain relation. Furthermore, from thermodynamic consideration (Aki 1980) we can have

$$c_{ijkl} = c_{klij} . \tag{2.29}$$

This condition will further reduce the number of independent elastic constants in the generalized stress-strain relation to 21.

Now let us consider the case in which the elastic medium under consideration is homogenous and isotropic. By isotropy we mean that the elastic properties of the medium are independent of the orientation of the coordinate axis. Thus, the coefficients c_{ijkl} remain invariant with respect to coordinate rotation. Under this condition the number of essential elastic constants reduces to 2, Therefore, for isotropic, homogenous and linearly elastic material the constitutive equation for the stress can be written as

$$\tau_{ij} = \lambda\theta\delta_{ij} + 2\mu e_{ij} . \tag{2.30}$$

Where λ and μ are Lame' constants and δ_{ij} the Kronecker delta symbol. Lame' constants are related to the Young's modulus, E, and Poisson's ratio, σ , by

$$\lambda = \frac{E\sigma}{(1+\sigma)(1-2\sigma)} \tag{2.31}$$

and $$\mu = \frac{E}{2(1+\sigma)} \quad . \tag{2.32}$$

2.2 Cauchy's equation of motion and elastic waves

The traction (surface force), body force and acceleration that act throughout a body with volume V and surface S must satisfy a constraint. This constraint is that the rate of change of momentum of particles constituting the body must be equal to the forces acting on the particles. From the development so far this can be stated in the following component form.

$$\int_S \tau_{ji}\, n_j \, ds + \int_V f_i \, dv = \int_V \rho\, u_{i,tt} \, dv. \tag{2.33}$$

Where τ_{ij} is the component of the stress and f_i is the component of body force per unit volume. Using Gauss' theorem this reduces to

$$\tau_{ji,j} + f_i = \rho\, u_{i,tt}. \tag{2.34}$$

Eq. (2.34) is Cauchy's first law of motion. Using eqs. (2.6) and (2.30) we can write

$$\tau_{ji} = \lambda u_{i,i}\, \delta_{ij} + \mu u_{i,j} + \mu u_{j,i}. \tag{2.35}$$

Substituting eq. (2.35) into eq. (2.34) gives

$$(\lambda u_{i,i}\, \delta_{ij} + \mu u_{i,j} + \mu u_{j,i})_{,j} + f_i = \rho\, u_{i,tt} \quad . \tag{2.36}$$

In the absence of body forces (the case we will be dealing with) eq. (2.36) reduces to

$$(\lambda u_{i,i}\, \delta_{ij} + \mu u_{i,j} + \mu u_{j,i})_{,j} = \rho\, u_{i,tt} \quad . \tag{2.37}$$

This expression implies

$$(\lambda+\mu)\, u_{j,ji} + \mu u_{i,jj} = \rho u_{i,tt} \,. \qquad (2.38)$$

Applying a standard method we write the displacement in terms of displacement potentials as follows (Achenbach 1975).

$$u_i = \varphi_{,i} + e_{ijk}\, \psi_{k,j} \,. \qquad (2.39)$$

Where e_{ijk} is the alternating tensor and φ and ψ are scalar and vector potentials.

Using eq. (2.39) the displacement-equation of motion, eq. (2.38), can be put in vector notation as

$$\mu\nabla^2(\vec{\nabla}\varphi + \vec{\nabla}\times\vec{\psi}) + (\lambda+\mu)\vec{\nabla}\vec{\nabla}\cdot(\vec{\nabla}\varphi + \vec{\nabla}\times\vec{\psi}) = \rho\frac{\partial^2}{\partial t^2}(\vec{\nabla}\varphi + \vec{\nabla}\times\vec{\psi}). \qquad (2.40)$$

Observing that $\vec{\nabla}\cdot\vec{\nabla}\times\vec{\psi} = 0$ and $\vec{\nabla}\cdot\vec{\nabla}\varphi = \nabla^2\varphi$ and rearranging we have

$$\vec{\nabla}(\rho\ddot{\varphi} - (\lambda+2\mu)\nabla^2\varphi) + \vec{\nabla}\times(\rho\ddot{\vec{\psi}} - \mu\nabla^2\vec{\psi}) = 0 \,. \qquad (2.41)$$

This expression is satisfied if

$$\rho\ddot{\varphi} = \rho\varphi_{,tt} = (\lambda+2\mu)\nabla^2\varphi = (\lambda+2\mu)\varphi_{,jj} \qquad (2.42)$$

and $$\rho\ddot{\vec{\psi}} = \vec{\psi}_{,tt} = \mu\nabla^2\vec{\psi} \,. \qquad (2.43)$$

These imply

$$\varphi_{,tt} = \alpha^2\varphi_{,jj} \qquad (2.44)$$

and $$\vec{\psi}_{,tt} = \beta^2\vec{\psi}_{,jj} \,, \qquad (2.45)$$

where $$\alpha^2 = \frac{\lambda+2\mu}{\rho} \,,$$

and $$\beta^2 = \mu/\rho \,.$$

Eqs. (2.44) and (2.45) are the required wave equations for dilatational and rotational waves with velocities α and β respectively.

2.3 Elastic surface waves

So far the development has been general. As a particular case, without lose of generality, let us consider a plane wave travelling in the X_1 direction and whose disturbance is largely confined to the neighbourhood of the free surface of an elastic half space. Let the X_3 axis be perpendicular to the direction of propagation and at any instant all particles in any line parallel to the X_2 axis have equal displacements. The above conditions assure that the partial derivatives with respect to X_2 vanish and the waves under consideration are surface waves. For this case, it is clear from eq. (2.38) that the displacement component , u_2, is not coupled with other displacement components. The vanishing of the partial derivatives with respect to X_2 gives

$$(\lambda+\mu)\, u_{j,j2} = 0. \tag{2.46}$$

Thus, eq. (2.38) reduces to

$$\mu u_{2,jj} = \rho u_{2,tt}$$

or
$$\beta^2 u_{2,jj} = u_{2,tt} \cdot \tag{2.47}$$

The other two components are coupled and they can be found from the solution of the uncoupled wave equations given in section 2.2. Therefore, for surface waves the wave equations can be written as

$$\alpha^2 \varphi_{,jj} = \varphi_{,tt} \quad , \tag{2.48}$$

$$\beta^2 \psi_{,jj} = \psi_{,tt} \qquad (\psi = \psi_2) \tag{2.49}$$

and $$\beta^2 u_{2,jj} = u_{2,tt} \, . \tag{2.50}$$

The general solutions for eqs. (2.48) - (2.50) are

$$\varphi = A_1 e^{ik(ct + rx_3 - x_1)} + A_2 e^{ik(ct - rx_3 - x_1)} \quad , \tag{2.51}$$

$$\psi = B_1 e^{ik(ct + sx_3 - x_1)} + B_2 e^{ik(ct - sx_3 - x_1)}, \tag{2.52}$$

and $$u_2 = D_1 e^{ik(ct + sx_3 - x_1)} + D_2 e^{ik(ct - sx_3 - x_1)} \tag{2.53}$$

respectively.

Where $$r = \left(\frac{c^2}{\alpha^2} - 1\right)^{1/2}$$

and $$s = \left(\frac{c^2}{\beta^2} - 1\right)^{1/2}$$

For the disturbance to be near the free surface, e^{iksx_3} and e^{ikrx_3} must diminish indefinitetly with increasing distance from the boundary. This means that e^{iksx_3} and e^{ikrx_3} must contain exponential factors in which the exponents are real and negative. Thus, r and s are taken to be imaginary.

Under the conditions mentioned at the beginning of this section, eq. (2.39) can be written componentwise for u_1 and u_3 as

$$u_1 = \varphi_{,1} - \psi_{,3} \tag{2.54}$$

and $$u_3 = \varphi_{,3} + \psi_{,1} \, . \tag{2.55}$$

Differentiation of eqs. (2.54) and (2.55) with respect to x_1 and x_3 respectively yields

$$u_{1,1} = \varphi_{,11} - \Psi_{,31} \qquad (2.56)$$

and $$u_{3,3} = \varphi_{,33} + \Psi_{,13} \cdot \qquad (2.57)$$

Noting that $u_{2,2} = \varphi_{,22} = 0$ and adding eqs. (2.56) and (2.57) give

$$\theta = u_{1,1} + u_{2,2} + u_{3,3} = \varphi_{,11} + \varphi_{,22} + \varphi_{,33} \cdot \qquad (2.58)$$

Thus, $$\theta = \varphi_{,ii} \cdot \qquad (2.59)$$

This shows that φ is associated with dilatational or P waves. Similarly it is possible to show that

$$u_{1,3} - u_{3,1} = \Psi_{,ii} \cdot \qquad (2.60)$$

Eq. (2.60) shows that Ψ is associated with rotational waves (vertically polarized shear waves, SV). u_2, a component of the displacement vector in the X_2 direction, is perpendicular to the direction of propagation. Thus it is associated with SH (horizontally polarized shear) waves.

Subsequently we will look at the formulation of Rayleigh wave (P and SV motion) dispersion in a multilayered medium with boundary condition.

CHAPTER III

RAYLEIGH WAVE DISPERSION IN A MULTILAYERED MEDIUM

3.1 Brief survey of the problem.

Problems related to the propagation of surface waves in an inhomogenous semi-infinite medium whose inhomogeniety varies only in one direction, can be treated by considering the inhomogenous medium to be approximated by a stack of, say n, parallel and homogenous layers (including the half space) in welded contact.

For surface waves of Rayleigh type the boundary conditions, continuity of stress and displacement at each interior interface and vanishing of stress at the free surface, in general constitute $4n - 2$ equations which can be expressed in matrix form. Thomson (1950) has derived such a matrix formulation for solving problems related to elastic waves propagating in a layered medium. Haskell (1953) corrected and systematized this method.

However, the solution of the period equation obtained from Haskell's method has computational difficulties. Knopoff (1964) and Dunkin (1965) have overcome these computational difficulties inherent to Haskell's method by suitable matrix formulation. Dunkin (1965) showed that for high frequencies the matrix components become large leading to inaccuracies in the solutions of the period equation. Experience has also shown that even for

moderate values of frequency, computations of the boundary conditions at large depths give wrong results.

Subsequently, we will closely follow Dunkin's approach in setting up the period equation and briefly discuss how the computational difficulties can be avoided.

The notations used upto now have facilitated the derivation of fundamental results of elasticity in compact form. Henceforth, we will follow the usual notations (u,v,w) and (x,y,z) instead of (u_1,u_2,u_3) and (x_1,x_2,x_3) respectively.

3.2 Matrix formulation of the problem for Rayleigh waves leading to the period equation.

We will consider a plane wave propagating in a semi-infinite medium made up of n parallel, homogenous, isotropic and elastic layers as shown in Figure 3.1. The positive x axis will be chosen as the direction of propagation.

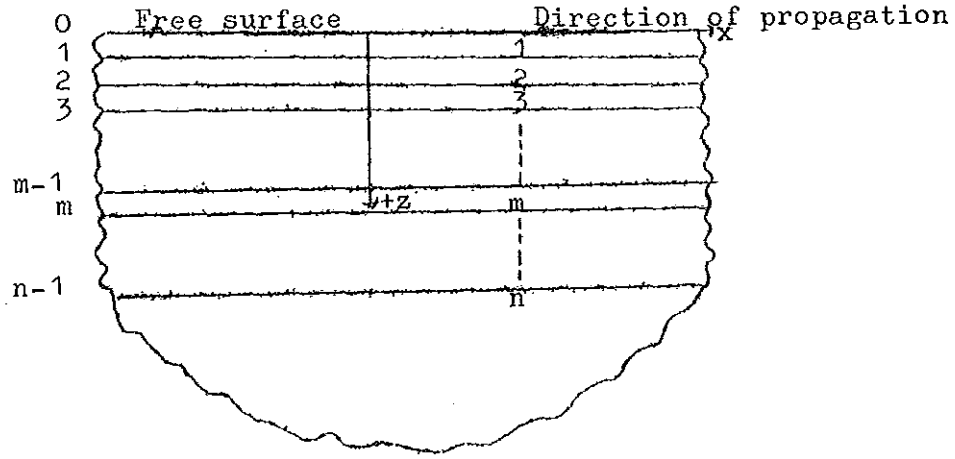

Fig. 3.1 Geometry of the elastic semi-infinite medium and numbering of layers and interfaces.

In a multilayered medium the condition of attenuation with depth of surface waves can be correctly accounted for by requiring

$$c < \beta_n \quad . \tag{3.1}$$

Where c is the phase velocity and β_n is the shear wave velocity in the n^{th} layer (see Figure 3.1).

The following parameters refer to the m^{th} layer in Figure 3.1.

λ_m, μ_m = Lame' elastic constants

ρ_m = density

α_m = compressional wave velocity

β_m = shear wave velocity

d_m = layer thickness

u_m = displacement component in the x direction

w_m = displacement component in the z direction

$\tau_{zz}^{(m)}$ = normal stress

$\tau_{zx}^{(m)}$ = shearing stress

The relevant displacement functions for the m^{th} layer are

$$u_m = \varphi_{m,x} - \psi_{m,z} \tag{3.2}$$

and

$$w_m = \varphi_{m,z} + \psi_{m,x} \quad . \tag{3.3}$$

Where φ_m and ψ_m are solutions of

$$\alpha_m^2 \, \varphi_{m,ii} = \varphi_{m,tt} \tag{3.4}$$

and $$\beta_m^2 \, \Psi_{m,ii} = \Psi_{m,tt} \qquad (3.5)$$

respectively.

In the following we will discuss a suitable matrix formulation of the problem by introducing the Laplace-Fourier transform defined by

$$f(x,z,t) = \frac{1}{4\pi^2 i} \int_{c_o - i\infty}^{c_o + i\infty} \int_{-\infty}^{\infty} f^*(\xi, z, s) \, e^{st + i\xi x} \, d\xi \, ds \quad \ldots\ldots \quad (3.6)$$

$$\text{where } f^*(\xi, z, s) = \int_{-\infty}^{\infty} \int_{0}^{\infty} f(x,z,t) \, e^{-st - i\xi x} \, dt \, dx . \qquad (3.7)$$

Adopting this transform pair for the displacement potentials in eqs. (3.4) and (3.5) gives

$$\varphi_m(x,z,t) = \frac{1}{4\pi^2 i} \int_{c_o - i\infty}^{c_o + i\infty} \int_{-\infty}^{\infty} \varphi_m^*(\xi, z, s) \, e^{st + i\xi x} \, d\xi ds \quad \ldots \quad (3.8)$$

$$\text{where } \varphi_m^*(\xi, z, s) = \int_{-\infty}^{\infty} \int_{0}^{\infty} \varphi_m(x,z,t) \, e^{-st - i\xi x} \, dt \, dx \quad \ldots \quad (3.9)$$

$$\text{and } \Psi_m(x,z,t) = \frac{1}{4\pi^2 i} \int_{c_o - i\infty}^{c_o + i\infty} \int_{-\infty}^{\infty} \Psi_m^*(\xi, z, s) \, e^{st + i\xi x} \, d\xi \, ds \quad \ldots \quad (3.10)$$

$$\text{where } \Psi_m^*(\xi, z, s) = \int_{-\infty}^{\infty} \int_{0}^{\infty} \Psi_m(x,z,t) \, e^{-st - i\xi x} \, dt \, dx . \qquad (3.11)$$

From eq. (3.8) we write

$$\varphi_{m,xx} = \frac{1}{4\pi^2 i} \int_{c_o - i\infty}^{c_o + i\infty} \int_0^\infty -\zeta^2 \phi_m(\zeta, z, s) e^{st + i\zeta x} d\zeta ds. \quad (3.12)$$

Similar expressions can be found for $\varphi_{m,zz}$ and $\varphi_{m,tt}$ and on substitution eq. (3.4) gives

$$\frac{\alpha_m^2}{4\pi^2 i} \int_{c_o - i\infty}^{c_o + i\infty} \int_0^\infty (-\zeta^2 \phi^*_m + \phi^*_{m,zz}) e^{st + i\zeta x} d\zeta ds$$

$$= \frac{1}{4\pi^2 i} \int_{c_o - i\infty}^{c_o + i\infty} \int_0^\infty s^2 \phi^*_m e^{st + i\zeta x} d\zeta ds , \quad (3.13)$$

which reduces to

$$\phi^*_{m,zz} - \left(\zeta^2 + \frac{s^2}{\alpha_m^2}\right) \phi^*_m = 0 . \quad (3.14)$$

Similarly eq. (3.5) yields

$$\psi^*_{m,zz} - \left(\zeta^2 + \frac{s^2}{\beta_m^2}\right) \psi^*_m = 0 . \quad (3.15)$$

Eqs. (3.14) and (3.15) are second order differential equations whose solutions are

$$\phi^*_m = C_m e^{h_m(z - z_{m-1})} + D_m e^{-h_m(z - z_{m-1})} = \phi^{*+}_m + \phi^{*-}_m \quad (3.16)$$

and $\psi^*_m = E_m e^{k_m(z - z_{m-1})} + F_m e^{-k_m(z - z_{m-1})} = \psi^{*+}_m + \psi^{*-}_m \quad (3.17)$

respectively.

Where $$h_m^2 = \xi^2 + \frac{s^2}{\alpha_m^2},$$

$$k_m^2 = \xi^2 + \frac{s^2}{\beta_m^2}$$

and z_{m-1} is the value of z at the $(m-1)^{th}$ interfsce.

The displacement functions u_m and w_m as given by eqs. (3.2) and (3.3) can also be written in transformed forms as

$$u_m^* = i\xi \varphi_m^+ - k_m \psi_m^+ + i\xi \varphi_m^- + k_m \psi_m^- \qquad (3.18)$$

$$w_m^* = h_m \varphi_m^+ + i\xi \psi_m^+ - h_m \varphi_m^- + i\xi \psi_m^- \ . \qquad (3.19)$$

For the case under consideration, the stress components involved are

$$\tau_{zz}^{(m)} = \lambda_m \Theta_m + 2\mu_m w_{m,z} \qquad (3.20)$$

and $$\tau_{zx}^{(m)} = \mu_m (u_{m,z} + w_{m,x}) \ , \qquad (3.21)$$

where $$\Theta_m = u_{m,x} + w_{m,z} \ . \qquad (3.22)$$

Using eq. (3.22) eq. (3.20) can be written as

$$\tau_{zz}^{(m)} = \lambda_m (u_{m,x} + w_{m,z}) + 2\mu_m w_{m,z} \qquad (3.23)$$

and in terms of displacement potentials this is

$$\tau_{zz}^{(m)} = \lambda_m (\varphi_{m,xx} + \varphi_{m,zz}) + 2\mu_m (\varphi_{m,zz} + \psi_{m,zx}) \qquad (3.24)$$

which reduces to

$$\tau_{zz}^{(m)*} = \lambda_m(-\xi^2\varphi_m^* + \varphi_{m,zz}^*) + 2\mu_m(\varphi_{m,zz}^* + i\xi\psi_{m,z}^*) \quad (3.25)$$

in transformed form. Using eqs. (3.16) and (3.17) we can have

$$\tau_{zz}^{(m)*} = (-\xi^2\lambda_m + h_m^2(\lambda_m + 2\mu_m))\varphi_m^{*+} + (-\xi^2\lambda_m + h_m^2(\lambda_m + 2\mu_m)) + 2\mu_m i\xi k_m \psi_m^{*+} - 2\mu_m i\xi k_m \psi_m^{*-} . \quad (3.26)$$

But, $$\lambda_m + 2\mu_m = \alpha_m^2 \rho_m , \quad (3.27)$$

$$h_m^2 = \left(\xi^2 + \frac{s^2}{\alpha_m^2}\right) \quad (3.28)$$

and $$\lambda_m = \alpha_m^2 \rho_m - 2\mu_m . \quad (3.29)$$

Use of eqs. (3.27) - (3.29) helps to write eq. (3.26) as

$$\tau_{zz}^{(m)*} = (2\mu_m\xi^2 + s^2\rho_m)\varphi_m^{*+} + (2\mu_m\xi^2 + s^2\rho_m)\varphi_m^{*-} + 2\mu_m i\xi k_m \psi_m^{*+} - 2\mu_m i\xi k_m \psi_m^{*-} . \quad (3.30)$$

Replacing ρ_m by $\frac{\mu_m}{\beta_m^2}$ eq. (3.30) can be written as

$$\tau_{zz}^{(m)*} = \mu_m \ell_m \varphi_m^{*+} + 2\mu_m i\xi k_m \psi_m^{*+} + \mu_m \ell_m \varphi_m^{*-} - 2\mu_m i\xi k_m \psi_m^{*-}, \quad (3.31)$$

where $$\ell_m = 2\xi^2 + s^2/\beta_m^2 . \quad (3.32)$$

Similarly the transformed expression for the shear stress is

$$\tau_{zx}^{(m)*} = 2i\mu_m\xi h_m \varphi_m^{*+} - \mu_m \ell_m \varphi_m^{*+} - 2i\mu_m\xi h_m \varphi_m^{*-} - \mu_m \ell_m \varphi_m^{*-} \quad (3.33)$$

The relations (3.18), (3.19), (3.31) and (3.33) between the

transform of the displacement and stress components and that of the displacement potentials can be written concisely in the following form:

$$Q_m^*(z) = T_m \, A_m^*(z) \, , \tag{3.34}$$

where

$$T_m = \begin{bmatrix} i\xi & -k_m & i\xi & k_m \\ h_m & i\xi & -h_m & i\xi \\ \mu_m \ell_m & 2\mu_m i\xi k_m & \mu_m \ell_m & -2\mu_m i\xi k_m \\ 2i\mu_m \xi h_m & -\mu_m \ell_m & -2i\mu_m \xi h_m & -\mu_m \ell_m \end{bmatrix}, \tag{3.35}$$

$$Q_m^* = \left[u_m^*, \; w_m^*, \; \tau_{zz}^{(m)^*} \, , \; \tau_{zx}^{(m)^*} \right] \tag{3.36}$$

and $$A_m^*(z) = \left[\phi_m^{*+}(z) \, , \psi_m^{*+}(z) \, , \phi_m^{*-}(z) \, , \psi_m^{*-}(z) \right] . \tag{3.37}$$

Furthermore, $$T_m^{-1} \; Q_m^*(z) = A_m^*(z) \, , \tag{3.38}$$

where

$$T_m^{-1} = \frac{\beta_m^2}{2\mu_m h_m k_m s^2} \begin{bmatrix} 2i\mu_m \xi h_m k_m & \mu_m \ell_m k_m & h_m k_m & i\xi k_m \\ -\mu_m \ell_m h_m & 2i\mu_m \xi h_m k_m & i\xi h_m & -h_m k_m \\ 2i\mu_m \xi h_m k_m & -\mu_m \ell_m k_m & h_m k_m & -i\xi k_m \\ \mu_m \ell_m h_m & 2i\mu_m \xi h_m k_m & -i\xi h_m & -h_m k_m \end{bmatrix} . \tag{3.39}$$

Using eq. (3.34) it is possible to write the following expression for the m^{th} layer.

$$Q_m^*(z_{m-1}) = T_m \, A_m^*(z_{m-1})$$

$$= T_m \begin{bmatrix} C_m e^{h_m(z_{m-1} - z_{m-1})} \\ E_m e^{k_m(z_{m-1} - z_{m-1})} \\ D_m e^{-h_m(z_{m-1} - z_{m-1})} \\ F_m e^{-k_m(z_{m-1} - z_{m-1})} \end{bmatrix}$$

$$Q_m^*(z_{m-1}) = T_m \begin{bmatrix} C_m \\ E_m \\ D_m \\ F_m \end{bmatrix} = T_m A_m^*(z_{m-1}) \, . \qquad (3.40)$$

Eq. (3.40) shows that

$$A_m^*(z_{m-1}) = \begin{bmatrix} C_m \\ E_m \\ D_m \\ F_m \end{bmatrix} \, . \qquad (3.41)$$

Similarly

$$Q_m^*(z_m) = T_m A_m^*(z_m) = T_m \begin{bmatrix} C_m e^{h_m(z_m - z_{m-1})} \\ E_m e^{k_m(z_m - z_{m-1})} \\ D_m e^{-h_m(z_m - z_{m-1})} \\ F_m e^{-k_m(z_m - z_{m-1})} \end{bmatrix} \qquad (3.42)$$

$$\text{or } Q^*_m(z_m) = T_m A^*_m(z_m) = T_m \begin{bmatrix} C_m e^{h_m d_m} \\ E_m e^{k_m d_m} \\ D_m e^{-h_m d_m} \\ F_m e^{-k_m d_m} \end{bmatrix} . \qquad (3.43)$$

Where $d_m = z_m - z_{m-1}$.

Therefore, we can write

$$A^*_m(z_m) = \begin{bmatrix} e^{h_m d_m} & 0 & 0 & 0 \\ 0 & e^{k_m d_m} & 0 & 0 \\ 0 & 0 & e^{-h_m d_m} & 0 \\ 0 & 0 & 0 & e^{-k_m d_m} \end{bmatrix} \begin{bmatrix} C_m \\ E_m \\ D_m \\ F_m \end{bmatrix} . \qquad (3.44)$$

Using eq. (3.41) eq. (3.44) gives

$$A^*_m(z_m) = E_m A^*_m(z_{m-1}) \quad . \qquad (3.45)$$

Where

$$E_m = \begin{bmatrix} e^{h_m d_m} & 0 & 0 & 0 \\ 0 & e^{k_m d_m} & 0 & 0 \\ 0 & 0 & e^{-h_m d_m} & 0 \\ 0 & 0 & 0 & e^{-k_m d_m} \end{bmatrix} . \qquad (3.46)$$

To relate the displacement and stress components at the free surface to the stress and displacement components at the

top of the half space we use boundary conditions which are:

1. Continuity of displacement and stress at an internal boundary, i.e.,

$$Q^*_m(z_m) = Q^*_{m+1}(z_m) \ . \tag{3.47}$$

2. Stress and displacement components at the free surface and just below the free surface should be equal, i.e.,

$$Q^*_1(0) = Q^*_0 \ . \tag{3.48}$$

3. No disturbance at infinity or $z = \infty$, i.e.,

$$\varphi^*_n = \psi^*_n = 0 \ . \tag{3.49}$$

From eq. (3.34) the first boundary condition can be written as

$$Q^*_{m+1}(z_m) = T_m A^*_m(z_m) \ . \tag{3.50}$$

Using eq. (3.45) eq. (3.50) can be expressed in the form

$$Q^*_{m+1}(z_m) = T_m E_m A^*_m(z_{m-1}) \ . \tag{3.51}$$

Applying eq. (3.38) reduces eq. (3.51) to

$$Q^*_{m+1}(z_m) = T_m E_m T_m^{-1} Q^*_m(z_{m-1}) \tag{3.52}$$

or

$$Q^*_{m+1}(z_m) = G_m Q^*_m(z_{m-1}) \ , \tag{3.53}$$

where

$$G_m = T_m E_m T_m^{-1} \ . \tag{3.54}$$

From eq. (3.53) it is clear that the matrix G_m equates the stresses and displacements at the m^{th} interface to the stresses and displacements at the $(m-1)^{th}$ interface. By repeated application of eq. (3.53) the solution can be continued from

the top surface through the intervening layers to the n^{th} layer. This can be expressed mathematically as

$$A_n^*(z_{n-1}) = T_n^{-1} G_{n-1} \cdots G_1 Q_0^* = RQ_0^* . \qquad (3.55)$$

Where R is a 4 x 4 matrix given by

$$R = T_n^{-1} G_{n-1} \cdots G_1 = \begin{bmatrix} r_{11} & r_{12} & r_{13} & r_{14} \\ r_{21} & r_{22} & r_{23} & r_{24} \\ r_{31} & r_{32} & r_{33} & r_{34} \\ r_{41} & r_{42} & r_{43} & r_{44} \end{bmatrix} . \qquad (3.56)$$

Now, R can be partitioned according to

$$R = \begin{bmatrix} R_{11} & R_{12} \\ R_{21} & R_{22} \end{bmatrix} . \qquad (3.57)$$

Then, eq. (3.55) can be written as

$$A_n^*(z_{n-1}) = RQ_o^* = \begin{bmatrix} R_{11} & R_{12} \\ R_{21} & R_{22} \end{bmatrix} \begin{bmatrix} \begin{pmatrix} u_o^* \\ w_o^* \end{pmatrix} \\ \begin{pmatrix} \tau_{zz}^{(o)*} \\ \tau_{zx}^{(o)*} \end{pmatrix} \end{bmatrix} . \qquad (3.58)$$

From the condition of radiation at infinity (third boundary condition) eq. (3.58) can be written as

$$\begin{bmatrix} \begin{pmatrix} 0 \\ 0 \end{pmatrix} \\ \begin{pmatrix} \dot{\psi}_n^* \\ \dot{\psi}_n^* \end{pmatrix} \end{bmatrix} = \begin{bmatrix} R_{11} & R_{12} \\ R_{21} & R_{22} \end{bmatrix} \begin{bmatrix} \begin{pmatrix} u_o^* \\ w_o^* \end{pmatrix} \\ \begin{pmatrix} \tau_{zz}^{(o)*} \\ \tau_{zx}^{(o)*} \end{pmatrix} \end{bmatrix} . \tag{3.59}$$

From this expression we obtain

$$R_{11} \begin{bmatrix} u_o^* \\ w_o^* \end{bmatrix} + R_{12} \begin{bmatrix} \tau_{zz}^{(o)*} \\ \tau_{zx}^{(o)*} \end{bmatrix} = \begin{bmatrix} 0 \\ 0 \end{bmatrix} . \tag{3.60}$$

This expression can be solved for the displacement components to yield

$$\begin{bmatrix} u_o^* \\ w_o^* \end{bmatrix} = -R_{11}^{-1} R_{12} \begin{bmatrix} \tau_{zz}^{(o)*} \\ \tau_{zx}^{(o)*} \end{bmatrix} . \tag{3.61}$$

From elementary theory of matrices

$$R_{11}^{-1} = \frac{(R_{11})^T}{\det R_{11}} \tag{3.62}$$

where $(R_{11})^T$ is the transpose of the cofactors of matrix R_{11}. Substitution of eq. (3.62) into eq. (3.61) gives

$$\begin{bmatrix} u_o^* \\ w_o^* \end{bmatrix} = - \frac{(R_{11})^T}{\det R_{11}} R_{12} \begin{bmatrix} \tau_{zz}^{(o)*} \\ \tau_{zx}^{(o)*} \end{bmatrix} . \tag{3.63}$$

At the free surface

$$\tau_{zz}^{(o)*} = \tau_{zx}^{(o)*} = 0 . \tag{3.64}$$

Therefore, for a nontrivial solution of eq. (3.63), it is

necessary to have

$$f(\xi, s) = \det R_{11} = 0 \quad , \tag{3.65}$$

where $s = iw$.

Eq. (3.65) is the required period equation.

3.3 Method of avoiding computational difficulties

If eq. (3.65) which is equivalent to Thomson-Haskell formulation is used as it is to obtain dispersion curves, the inherent computational difficulties will still be there. However, using eq. (3.54) eq. (3.56) can be written as

$$R = T_n^{-1} G_{n-1} \ldots T_m E_m T_m^{-1} \ldots G_1 \tag{3.66}$$

or $$R = A E_m B \quad , \tag{3.67}$$

where $$A = T_n^{-1} G_{n-1} \ldots G_{m+1} T_m \tag{3.68}$$

and $$B = T_m^{-1} \ldots G_1 \, . \tag{3.69}$$

Now, eq.(3.67) can be expanded in terms of the elements of the matrices involved as

$$\begin{bmatrix} r_{11} & r_{12} & r_{13} & r_{14} \\ r_{21} & r_{22} & r_{23} & r_{24} \\ r_{31} & r_{32} & r_{33} & r_{34} \\ r_{41} & r_{42} & r_{43} & r_{44} \end{bmatrix} = \begin{bmatrix} a_{11} & a_{12} & a_{13} & a_{14} \\ a_{21} & a_{22} & a_{23} & a_{24} \\ a_{31} & a_{32} & a_{33} & a_{34} \\ a_{41} & a_{42} & a_{43} & a_{44} \end{bmatrix} \begin{bmatrix} e^{h_m d_m} & 0 & 0 & 0 \\ 0 & e^{k_m d_m} & 0 & 0 \\ 0 & 0 & e^{-h_m d_m} & 0 \\ 0 & 0 & 0 & e^{-k_m d_m} \end{bmatrix}$$

$$\times \begin{bmatrix} b_{11} & b_{12} & b_{13} & b_{14} \\ b_{21} & b_{22} & b_{23} & b_{24} \\ b_{31} & b_{32} & b_{33} & b_{34} \\ b_{41} & b_{42} & b_{43} & b_{44} \end{bmatrix} . \qquad (3.70)$$

A general element of the product of these matrices can be written as

$$r_{ij} = r'_{ij} e^{h_m d_m} + r''_{ij} e^{k_m d_m} + r'''_{ij} e^{-k_m d_m} + r''''_{ij} e^{-k_m d_m} . \qquad (3.71)$$

. . .

The subdeterminant of R, i.e.,

$$\det R_{11} = r_{11} r_{22} - r_{12} r_{21} \qquad (3.72)$$

can be evaluated by substituting for r_{ij} from eq. (3.71). The resulting expression will contain products of like exponentials in the form $e^{2h_m d_m}$, etc. so that we can write

$$\det R_{11} = e^{2h_m d_m} (r'_{11} r'_{22} - r'_{12} r'_{21}) + \text{other terms} . \qquad (3.73)$$

Now let us consider the case in which h_m becomes large and positive. Under this condition, the first term in eq. (3.73) becomes dominant unless

$$r'_{11}\, r'_{22} = r'_{12}\, r'_{21} . \tag{3.74}$$

From eq. (3.73) it is clear that, if one computes first components of R_{11} and then det R_{11}, products of like exponentials cannot be eliminated. This large value leads to roundoff error which in turn leads to obtaining inaccurate results and computational difficulties. To avoid the difficulties it is useful to write det R_{11}, which is essentially a determinant of two by two matrix, as a product of the subdeterminants of the individual matrices (see Appendix A) as

$$\det R_{11} = r \begin{vmatrix} 12 \\ 12 \end{vmatrix} = t^{n} \begin{vmatrix} 12 \\ ab \end{vmatrix} g^{n-1} \begin{vmatrix} ab \\ cd \end{vmatrix} \cdots g^{1} \begin{vmatrix} ef \\ 12 \end{vmatrix} , \tag{3.75}$$

where $t^{n} \begin{vmatrix} 12 \\ ab \end{vmatrix}$ are subdeterminants of T_n^{-1} and

$g^{n-1} \begin{vmatrix} ab \\ cd \end{vmatrix}, \ldots, g^{1} \begin{vmatrix} ef \\ 12 \end{vmatrix}$ are subdeterminants of the G_m matrices.

The next stage is to show that products of like exponentials will not be present in the subdeterminants of the G matrices (see Appendix A) thereby the dominant term, $e^{h_m d_m} \times e^{h_m d_m} = e^{2h_m d_m}$ doesn't arise. The nonvanishing term in the product of subdeterminants is

$$g^{m} \begin{vmatrix} ij \\ kl \end{vmatrix} = t^{m} \begin{vmatrix} ij \\ ab \end{vmatrix} t^{m} \begin{vmatrix} ab \\ kl \end{vmatrix} e^{m} \begin{vmatrix} ab \\ ab \end{vmatrix}, \quad (a < b). \tag{3.76}$$

A glance at eq. (3.39) shows that there is no exponential term involved in $t^{n} \begin{vmatrix} 12 \\ ab \end{vmatrix}$ of eq. (3.75). Therefore, if one starts the computation of the period equation with

algebric expressions of the subdeterminants of the G_m matrices, products of like exponentials don't occur and computational difficulties associated with them don't arise.

In this study, a program written for the period equation expressed as subdeterminants of the G_m matrices is used to generate theoretical modes. The algebric expressions of these subdeterminants are given in Appendix B.

CHAPTER IV

METHODS

In the preceding chapters we have introduced the problem we will be dealing with and discussed the theoretical basis for surface wave dispersion so that for a given earth model we have a means of generating theoretical dispersion curves. Our main concern, however, is the interpretation of dispersion curves as found from seismograms of earthquake waves that have travelled along paths cited in chapter I. The identification of wave types, especially Rayleigh wave and the production of dispersion curves in light of possible modal contribution, using seismogram data will be the task of this chapter.

4.1 The data

It is mentioned in chapter I that three events with different station-epicenter azimuths are considered for this study. Location of epicenters and their origin times are taken from the US Geological Survey's Earthquake Data Report. The following table gives the relevant parameters of the events.

Table 2 Date and relevant parameters of the events.

Date						
Dec.12/1968	17:30:31.9	12.087N	45.867E	W.Gulf of Aden	4.6	850.586 km
Mar. 5/1980	03:12: 5.2	16.610N	40.239E	Red Sea	-	852.220 km
Mar.24/1969	11:54:15.5	27.592N	33.829E	Arab Rep of Egypt	5.2	2109.220 km

4.2 Identification of wave - type

For the analysis of Rayleigh waves vertical component seismograms from the Addis Ababa seismic station (AAE) are utilized. This is a standard station (WWSSN) with periods of seismometer and galvanometer 15 and 100 seconds respectively.

Figures 4.1, 4.2, and 4.3 show records of Rayleigh wave trains for the paths: Western Gulf of Aden - Addis Ababa (GOA - AAE), Red Sea - Addis Ababa (RES - AAE) and Arab republic of Egypt - Addis Ababa (ARE - AAE) respectively.

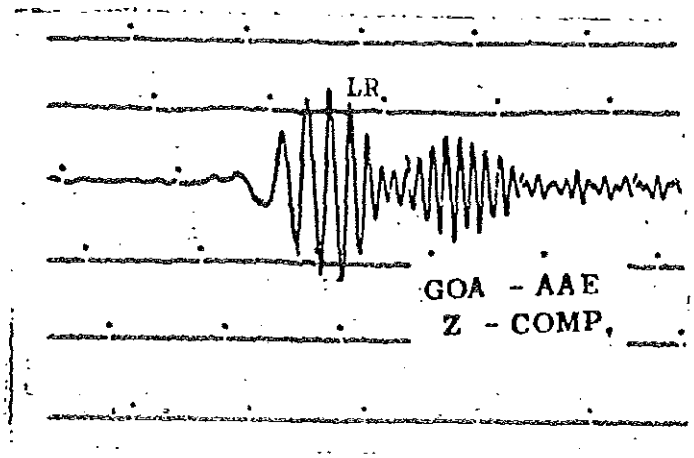

Fig. 4.1 Record of Rayleigh wave train for GOA - AAE path.

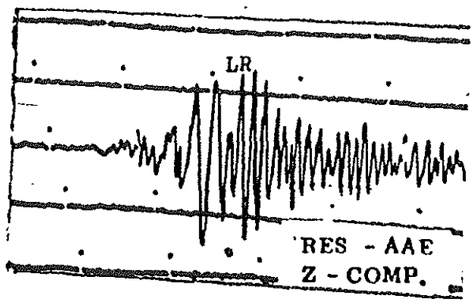

Fig. 4.2 Record of Rayleigh wave train for RES - AAE path.

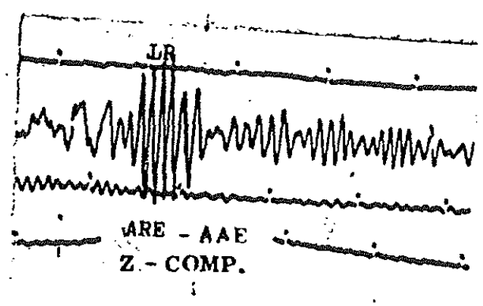

Fig. 4.3 Record of Rayleigh wave train for ARE - AAE path.

For each of the paths particle motion is used to identify Rayleigh waves. It is evident that for the paths RES - AAE and ARE - AAE, which are due north, the motion is retrograde elliptical as found from plots of Z versus NS amplitudes with the same time base. For the GOA - AAE path, which is due east of the recording station, the particle motion is retrograde elliptical as found from plot of Z versus EW component.

Figures 4.4, 4.5 and 4.6 show particle motion of Rayleigh wave for GOA - AAE , RES - AAE and ARE - AAE respectively.

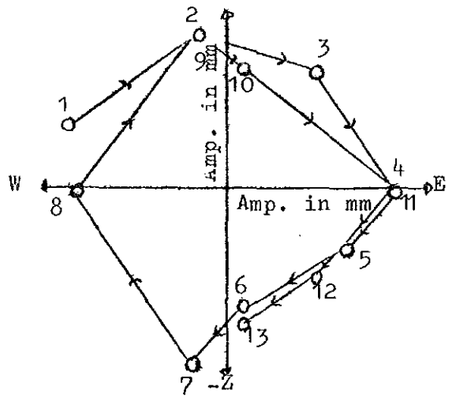

Fig. 4.4 Rayleigh wave - particle motion for GOA - AAE path.

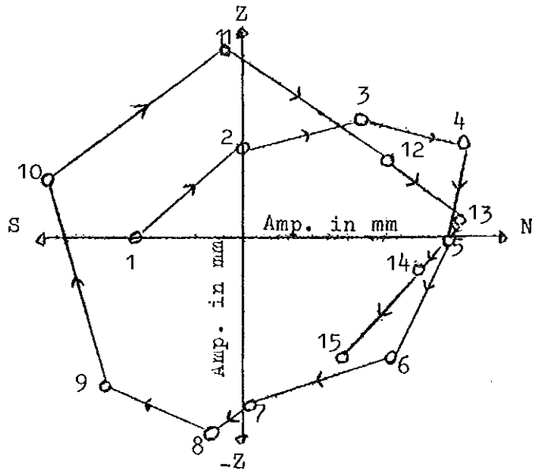

Fig. 4.5 Rayleigh wave - particle motion for RES - AAE path.

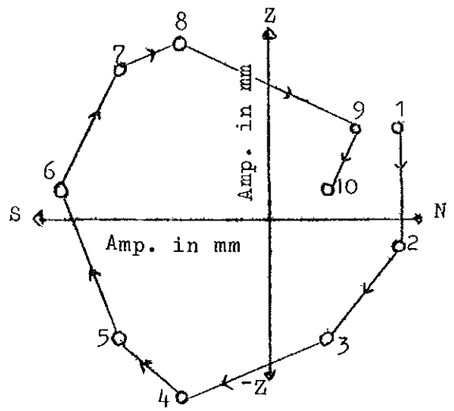

Fig. 4.6 Rayleigh wave - particle motion for ARE - AAE path.

4.3 Correction

Before determining group velocities it is necessary to make corrections for group time delay due to instrumental response and path effect. For group time delay a table (A. Douglas, personal communication) is used to correct travel times for different periods. The relevant periods and corresponding delay times are shown in Table 3.

Table 3 Period versus group time delay (After A. Douglas).

Period in sec.	4.00000	5.00733	6.00600	7.01370	8.00000	9.02203	11.01075
Group time delay in sec.	0.28211	0.46165	0.69650	0.99817	1.36015	1.80264	2.80504

In addition to the above correction the effect of oceanic parts of the paths on group velocities must also be considered. For the GOA - AAE and RES - AAE paths the epicenters lie in the continental shelves of western Gulf of Aden and the Red Sea respectively where the water depths are less than 500 m as found from a bathymetric chart. Following numerous other workers who have considered similar depths of water, for example, Tryggvason (1962) and Payo (1967), we have ignored oceanic correction for these paths. The ARE - AAE path is a totaly continental path.

4.4 Mode resolution and methods used to obtain dispersion curves from seismograms

Regarding seismogram analysis for dispersion the most difficult problem is related to separation of modes. The longest epicentral distance for the events under consideration is about 2000 km while the shortest is less than 1000 km. Therefore, the events as recorded at AAE are of short epicentral distances. Hence, the mode problem can arise in the analysis of the seismograms.

Landisman et al. (1969) studied the problem of mode separation at long periods in which he applied a moving window analysis. From outcomes of experiments other workers, for example Pfeffer and Zarichny (1963) have found that insufficient resolution results at long periods if a fixed window is utilized. In the moving window analysis different window widths for different periods are used to maintain the same relative frequency resolution at all periods in evaluation of amplitudes. The instantaneous amplitude in db is then plotted as a function of group velocity and period (those periods evenly spaced along a log - periodic scale). From the contoured display the presence of different modes can be inferred. Aki (1980) has recommended this method for resolving modes.

It is stated (Landisman et al. 1969) that good result are not obtained at very long and short periods when the moving

window method is used. As definite values are not given for short periods at which this problem arises we will consider both moving and fixed windows to analyse our data. It will be shown that for the period range considered here both moving and fixed windows give similar results.

Following Landisman et al. (1969) a cosine squared window function of the form

$$W(t) = \begin{cases} \cos^2 \left(\frac{\pi t}{WT_m}\right) & \text{for } |t| \leq \tfrac{1}{2}WT_m \\ 0 & \text{for } |t| > \tfrac{1}{2}WT_m \end{cases}, \qquad (4.1)$$

where W = ratio of window length to the period of analysis and T_m = the current period of analysis, is used. The parameter W is assigned a value of 4 for the analysis presented in this study.

Making the center of the window coincide with arrival times of equally spaced group velocities, the windowed data is Fourier analysed using the Fourier transform given by

$$F(w) = \int_{-\frac{1}{2}WT_m}^{\frac{1}{2}WT_m} w(t) \; f(t) \; e^{-iwt} \, . \qquad (4.2)$$

Evaluation of the integral is performed using descrete Fourier transform (Brigham 1974) given by

$$F_{\left(\frac{n}{NT}\right)} = \sum_{k=0}^{N-1} F(KT) \; e^{\frac{-2i\pi nk}{N}} \, , \qquad (4.3)$$

where f(KT) are the windowed data,

N is the number of prepared samples,

T is the sampling interval

and n and k are running indices. In this case n, N and T are fixed numbers. The instantaneous amplitudes in db as a function of period and group velocity are displayed and contoured. From the contoured display, modes are inferred.

On the other hand, as observed from seismograms the period under study are not long (the shortest period Landisman et al. (1969) considered is almost equal to the longest period observed here on the seismograms). Therefore, following the argument given earlier the data prepared for the different paths are windowed by a fixed window length of cosine squared window function,

$$W(t) = \begin{cases} \cos^2 \dfrac{\pi t}{2P} & \text{for } 0 \leq |t| \leq P \\ 0 & \text{for } |t| > P \end{cases} , \quad (4.4)$$

where P is the period. Taking the center of the window to be the arrival times of equally spaced group velocities, the windowed data is Fourier analysed as before using

$$F\left(\frac{n}{NT}\right) = \sum_{k=0}^{N-1} f(KT) \; e^{\frac{-i2\pi nk}{N}} , \quad (4.5)$$

where T is the sampling interval as before,

N is the number of prepared samples,

f(KT) are the windowed data

and n, k = 0, 1, . . . , N-1 .

However, in this case N and T are fixed numbers. A computer program flow chart for this is given in Appendix C.

For this case also the instantaneous amplitudes in db as a function of period and group velocity are displayed and modes are inferred from the contoured display.

For both moving and fixed windows different modes could be inferred by drawing lines through the maxima of the contours. In the next section we will consider the allied problem of generating theoretical modes.

4.5 Generating theoretical modes.

In generating theoretical modes compressional wave velocity, layer thickness and Poisson's ratio were taken as independent variables. Once a compressional wave velocity is chosen for a layer, the density of that layer is fixed by using the Nafe-Drake curve (Talwani et al. 1959). The Poisson's ratio and compressional wave velocity of the layer will further determine the shear wave velocity through the relation

$$\beta = \alpha \sqrt{\frac{1 - 2\sigma}{2(1 - \sigma)}} \quad . \tag{4.6}$$

In fitting theoretically generated dispersion curves to dispersion curves obtained from seismograms the independent variables cited above are varied within limits obtained from other geophysical works in the region.

A program written using Dunkin's formalism (Robert H. Herrmann, personal communication) is used to generate theoretical modes. Using this program, theoretical modes for more than 150 various models for all paths are generated.

CHAPTER V

DISCUSSION OF RESULTS AND CONCLUSIONS.

We have considered theoretical generation of dispersion curves for various modes for a given earth model. We have also seen methods of obtaining dispersion curves from seismograms in light of contribution by different modes.

In the following sections we will examine the results obtained for each path in turn in the light of recent geophysical works in seismic sounding, gravity and surface wave dispersion.

Hereafter, dispersion curves obtained from seismograms by peak and trough, fixed window Fourier analysis and moving window analysis will be referred to as "observed dispersion curves".

5.1 GOA - AAE path

This path traverses the southern part of the Afar Depression. The Rayleigh wave train identified for this path is composed of two modes, namely, the fundamental and first mode Rayleigh. The observed dispersion curves along with the theoretically generated dispersion curves for the accepted model are shown in Figures 5.1 and 5.2.

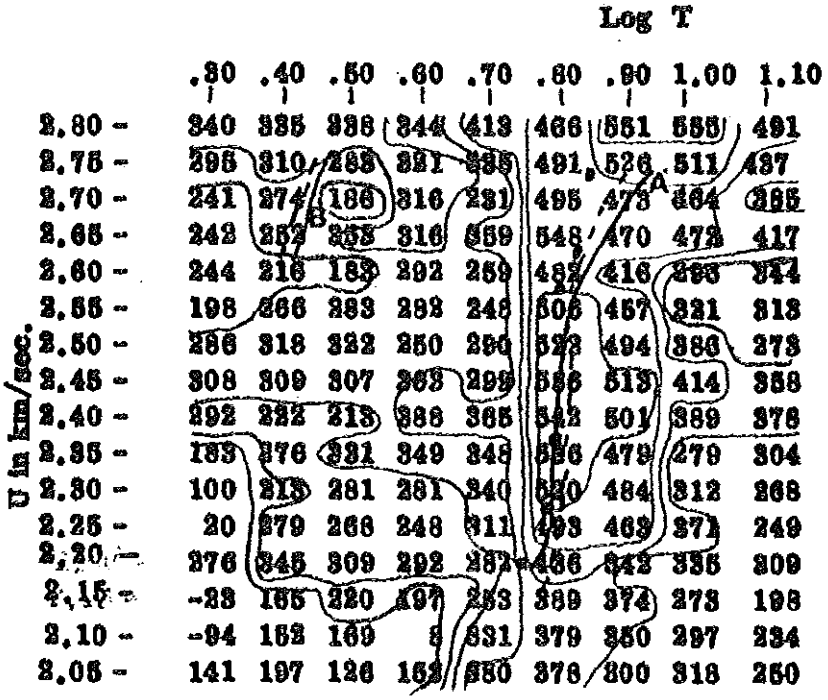

Fig. 5.1 **Dispersion curves for GOA - AAE path:** **(——) theory, (– – – –) fixed window Fourier analysis, (. . .) peak and trough method,** (A) Fundamental mode, (B) First mode.

Log T

U in km/sec.	.48	.55	.62	.69	.76	.83	.90	.97	1.04
2.90 –	313	322	359	389	421	441	523	670	589
2.85 –	266	340	378	382	412	481	537	569	621
2.80 –	278	78	316	351	393	473	535	542	542
2.75 –	187	268	300	341	431	482	508	513	511
2.70 –	207	331	293	337	409	452	458	449	264
2.65 –	126	295	280	326	393	433	382	337	472
2.60 –	189	255	298	342	412	442	419	364	296
2.55 –	301	286	280	343	423	466	423	461	321
2.50 –	262	352	322	250	444	486	251	475	386
2.45 –	301	377	364	392	459	449	511	430	414
2.40 –	259	385	376	428	482	507	500	397	389
2.35 –	284	391	342	382	467	512	428	424	279
2.30 –	212	265	333	382	442	443	482	422	312
2.25 –	218	132	276	349	442	457	458	448	371
2.20 –	200	151	256	298	389	411	396	300	336
2.15 –	102	210	245	255	325	342	370	299	273
2.10 –	97	141	109	189	210	326	351	288	304
2.05 –	140	233	283	328	370	362	311	273	298

Fig. 6.2 Dispersion curves for GOA - AAE path:
(——) theory, (– – – –) moving window analysis,
(. . .) peak and trough method. (A) Fundamental mode,
(B) First mode.

A brief glance at the figures shows that there is good agreement between the theoretical and observed dispersion curves.

Crustal models obtained from recent geophysical works along with that of this study are shown in Figure 5.3. As can be seen from Figure 5.3 the accepted crustal model for this study is represented by a three-layer crust 27 km thick overlying 4 km thick anomalous mantle with the proper mantle underneath.

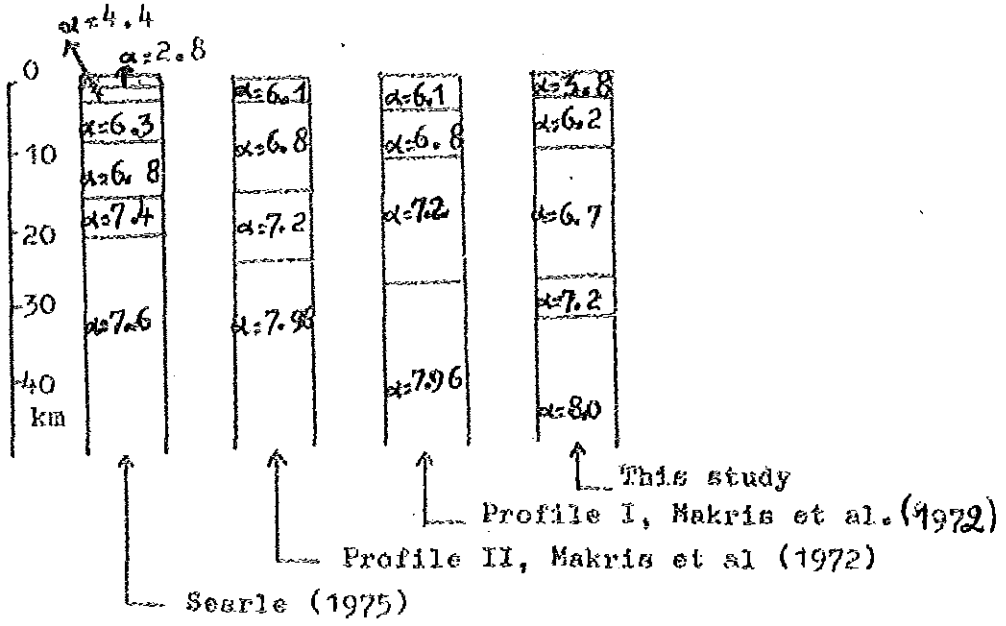

Fig. 5.3. Crustal models of southern Afar as found from recent geophysical works and this study.

Makris et al. (1972) have found crustal models for various orientations of profiles in the Afar Depression from gravity data. The path considered here crosses two of the profiles,

namely, profile I and II. The crustal models shown in Figure 5.3 for the profiles are taken at the points of intersection of these profiles with the GOA - AAE path. All parameters except the layer thickness are in good agreement with the results obtained in this study. The slight difference in layer thickness is due to differences in the orientation of propagation path and the orientation of profiles I and II. As can be seen from all the profiles of Makris et al. (1972) the anomalous mantle wedges out lying deeper under a thick crust as the escarpments are approached; whereas it is thicker and lies at shallow depths under a thin crust in central Afar.

The GOA - AAE path runs close to the escapments of the Afar Depression and this would imply a thicker crust as the accepted model suggests. This would be in agreement with the overall geometry of the anomalous - crust system.

Searle (1975) suggested a range of crustal models from dispersion study for a path (Tadjura - Addis Ababa) in southern Afar. No contribution by different modes was considered in preparing his dispersion curves. A crustal model of Searle is shown in Figure 5.3.

Jones (1968) also studied surface wave dispersion and obtained general results for paths between western Gulf of Aden and Addis Ababa.

The weighted mean Poisson's ratio for GOA - AAE path is found to be 0.274. This result is higher than the Poisson's

ratio for a normal continental crust which ranges from 0.25 - 0.26. Searle (1975) obtained Poisson's ratio as high as 0.29 for a path crossing a significant portion of a region where the Poisson's ratio could be even much higher, as high as 0.33, due to partial melting (Ruegg 1975). The relatively low Poisson's ratio we obtained is for a path which doesn't include known regions of partial melting.

5.2 RES - AAE path

As mentioned in chapter I no model from dispersion of surface waves has been suggested up to the present for this path. The observed dispersion curves along with the theoretical dispersion curve of the accepted model are shown in Figures 5.4 and 5.5.

U in Km/sec	Log T: .30	.40	.50	.60	.70	.80	.90	1.00	1.10
2.75 -	294	438	398	529	447	551	581	525	205
2.70 -	308	399	327	503	370	550	586	529	341
2.65 -	279	301	378	452	415	581	504	512	365
2.60 -	326	324	362	397	481	504	624	446	443
2.55 -	391	397	283	418	500	465	502	467	445
2.50 -	397	332	256	429	509	490	471	385	371
2.45 -	347	216	342	402	449	514	459	431	307
2.40 -	323	272	364	352	359	498	435	381	358
2.35 -	332	257	353	366	388	478	231	384	358
2.30 -	286	228	330	344	432	475	388	354	310
2.25 -	155	290	220	388	467	471	364	423	409
2.20 -	365	328	283	391	381	471	426	435	434
2.15 -	284	315	299	345	442	452	357	338	352

Fig. 5.4 Dispresion curves for RES - AAE path:
(———) theory, (- - - - - - -) fixed window Fourier analysis, (. . . .) peak and trough method,
(A) Fundamental mode, (B) First mode.

U in Km/sec.	Log T .48	.55	.62	.69	.76	.83	.90	.97	1.04
2.80 -	263	443	428	467	548	541	540	550	612
2.75 -	396	439	469	474	515	540	569	623	525
2.70 -	389	411	438	444	489	541	566	640	501
2.65 -	224	271	366	391	453	521	552	539	512
2.60 -	273	363	365	462	478	483	538	478	446
2.55 -	389	378	443	262	433	207	455	436	407
2.50 -	409	371	440	462	484	480	436	424	364
2.45 -	234	244	296	336	456	401	405	569	231
2.40 -	122	325	338	438	412	442	455	400	387
2.35 -	202	193	325	267	431	440	883	362	384
2.30 -	223	297	377	412	457	459	439	363	341
2.25 -	243	363	416	422	467	460	341	414	424
2.20 -	267	286	272	370	464	456	458	414	435
2.15 -	286	322	376	613	439	421	351	340	338

Fig. 5.5 Dispersion curves for RES -AAE path:
(_____) theory, (- - - - - -) moving window analysis
(. . . .) peak and trough method, (A) Fundamental mode, (B) First mode.

The accepted crustal model together with crustal models obtained by other geophysical workers are shown in Figure 5.6.

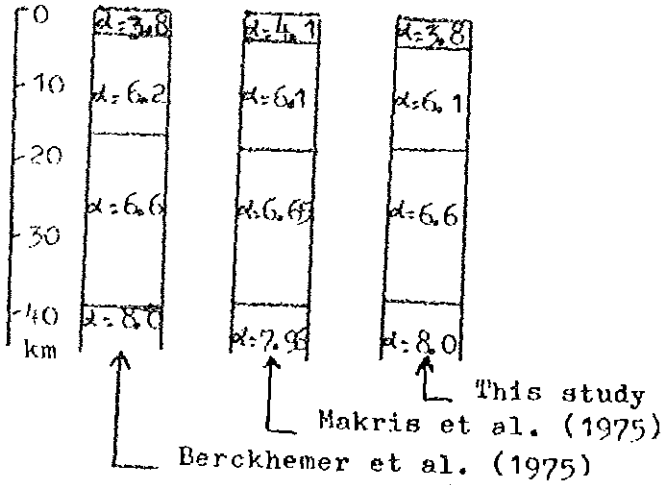

Fig. 5.6 Crustal models of Ethiopian highlands as found in this study and other geophysical works done earlier.

The good agreement of the theoretical and observed dispersion curves shown in Figures 5.4 and 5.5 suggests that the crustal structure along this path can be approximated by a three-layer crust with a mean crustal thickness of 37 km.

From a profile of seismic soundings on Ethiopian highlands Berckhemer et al. (1975) obtained a mean crustal thickness of the same order (see Figure 5.6).

Also, Makris et al. (1975) obtained from gravity data a mean crustal thickness of about 38 km with similar layer parameters as those obtained in this study.

From their study of travel time of near earthquakes Searle and Gouin (1971) estimated the mean crustal thickness of the Ethiopian plateau to be as high as 48 km. This value is higher than the value obtained in this study.

The weighted mean Poisson's ratio for this path is found to be 0.259. This value is in agreement with that of a normal continental crust.

5.3 ARE - AAE path

As mentioned in chapter I the only crustal model for this path is that of Sandos (Ph.D. Thesis, not yet published, personal communication), who approximated the crust by a single-layer model without considering modal contribution. He suggested a mean crustal thickness of 37 km for the Helwan - Addis Ababa path.

In this study modal contribution is considered and many theoretical modes are generated to obtain a good fit to the observed dispersion curves. Figures 5.7 and 5.8 show the identified modes and plots of observed dispersion curves along with the theoretical dispersion curves of the accepted model.

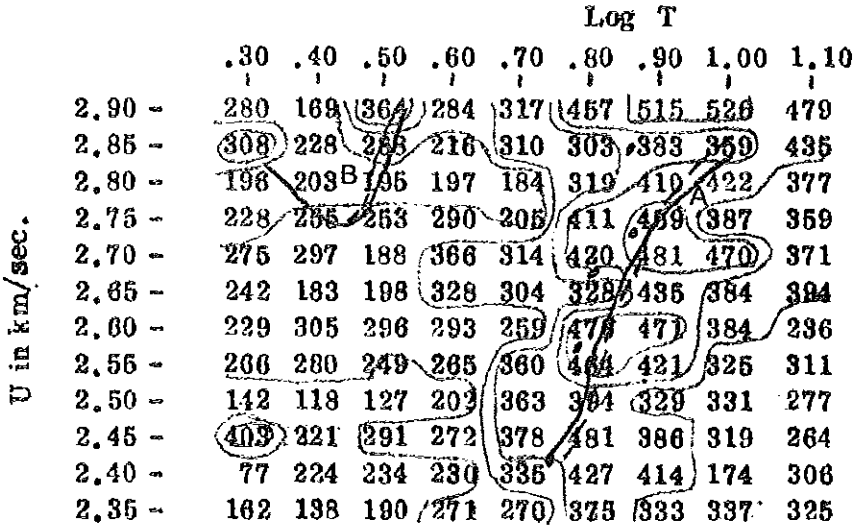

Fig. 5.7 Dispersion curves for ARE - AAE path: (_____) theory, (B- - - -) fixed window Fourier analysis, (. . . .) peak and trough method, (A) Fundamental mode (B) First mode.

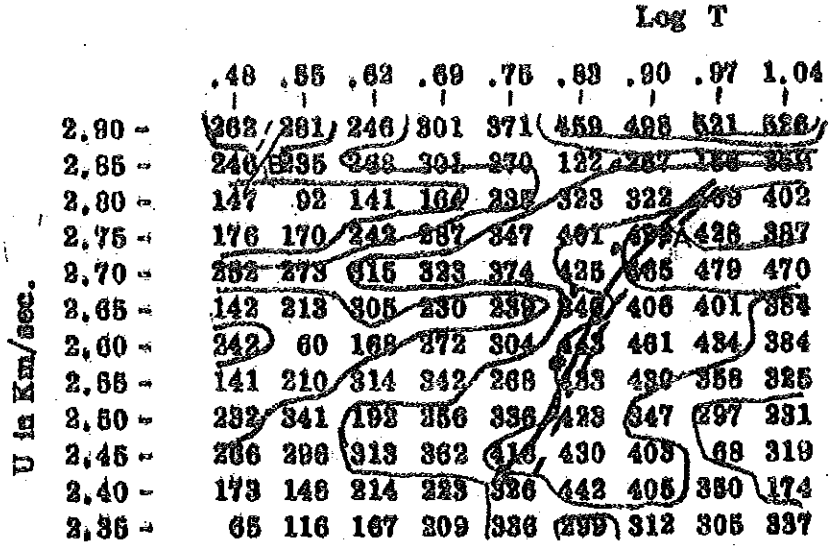

Fig. 5.8 Dispersion curves for ARE - AAE path: ( ) theory, (------) moving window analysis, (. . . .) peak and trough method. (A) Fundamental mode, (B) First mode.

The crustal model whose dispersion curves best fit to the observed dispersion curves along with that of Sandos and AFRIC model (Gumper and Pomeroy 1970) are shown in Figure 5.9

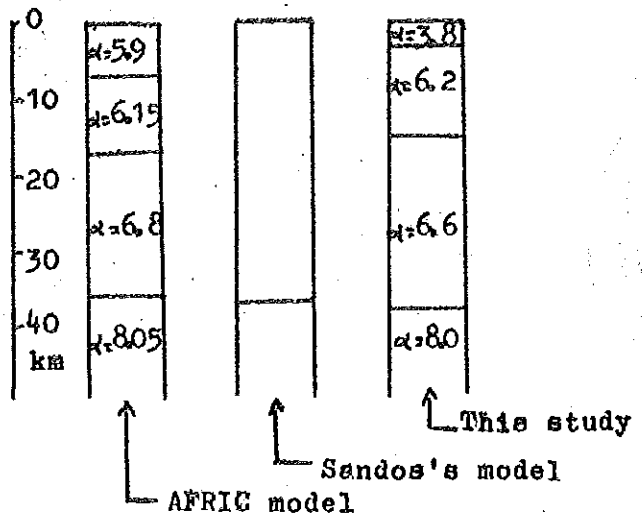

Fig. 5.9 Crustal models for ARE - AAE path and AFRIC model.

As can be seen from Figure 5.9 the crustal structure of the ARE - AAE path found in this study is approximated by a three-layer crust. The parameters of this model are similar to those of the RES - AAE path. For the ARE - AAE path a mean crustal thickness of 38 km is obtained and this is in agreement with that of Sandos.

The difference between the AFRIC modal (Gumper and Pomeroy 1970) and that obtained in this study can be wholly accounted for by the fact that the AFRIC model parameters are general and not restricted to certain regions and paths.

Here again, the weighted mean value of the Poisson's ratio is found to be in the range similar to that of a normal continental crust.

Considering the whole region under study, we can see from Figure 5.10 that the crustal structure below southern Afar and the ARE - AAE paths are thinner and thicker respectively as compared to that of the RES - AAE path. With the exception of thickness of layers, the crustal models obtained in this study have similar parameters for the GOA - AAE, RES - AAE and ARE - AAE paths.

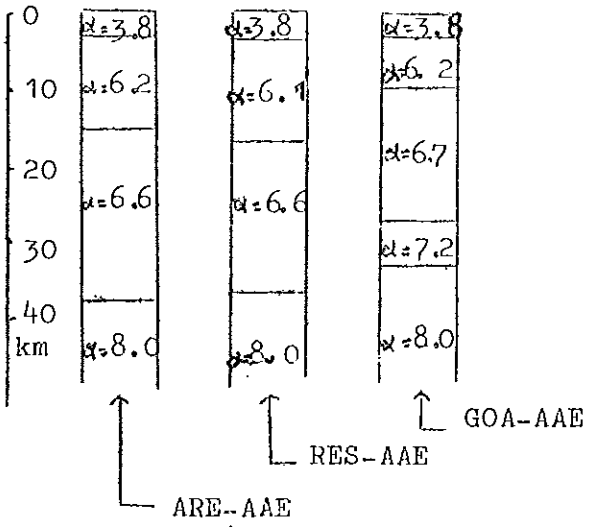

Fig. 5.10 Crustal models of the region under study.

5.4 Conclusions

1. This study (GOA - AAE path) has shown the possible presence of a thin layer of anomalous mantle near the margins of the Afar Depression. Furthermore, the relatively high Poisson's ratio obtained compared to that of a normal continental crust is consistent with the overall picture of the region.
2. The mean crustal thickness for RES - AAE path obtained in this study resolves the ambiguity in earlier results (for example, crustal thicknesses obtained from gravity data and near earthquake travel times). The value obtained (37 km) is in close agreement with those of Makris et al. (1975) and Berckhemer et al (1975).

3. The crustal structure of ARE - AAE path can be approximated by a three-layer model thereby improving the suggested single-layer model of Sandos.
4. Regarding the crustal models for the RES - AAE and ARE - AAE paths it can be suggested that there is no significant difference in the crustal structures of the two paths.
5. For the RES - AAE and ARE - AAE paths the crustal struc structures obtained are normal continental overlying normal mantle.
6. Production of dispersion curves from seismograms using methods of resolving modes rather than the simple peak and trough method has shown that better agreement with theoretical dispersion curves can be obtained. This indicates inherent multimode propagation which must be considered in the study of dispersion at short epicentral distances.
7. It has been shown (in all the three cases) that both moving window analysis and fixed window Fourier analysis give similar results thereby showing that moving window analysis is superfluous for the period range considered here.

APPENDIX A

THEOREM 1.

If P, D_1, D_2, . . .,D_n are matrices having a range of component indices of 2 or greater and

$$P = D_1 D_2 \cdots D_n$$

then, $P\begin{vmatrix} ij \\ kl \end{vmatrix} = d^1 \begin{vmatrix} ij \\ mn \end{vmatrix} d^2 \begin{vmatrix} mn \\ op \end{vmatrix} \cdots d^{n-1} \begin{vmatrix} st \\ uv \end{vmatrix} d^n \begin{vmatrix} uv \\ kl \end{vmatrix}$,

where the summed pairs of indices are to be only distinct pairs of distinct indices.

Proof :-

The proof will be given for $n = 3$. If one wants to have an expression for $n > 3$, one can write the expression by analogy to the case $n = 3$.

The determinant of a matrix P with rows i and j and column k and l can be defined as

$$P\begin{vmatrix} ij \\ kl \end{vmatrix} = P_{ik} P_{jl} - P_{il} P_{jk} \quad . \tag{A.1}$$

If P is a product of three (n=3) matrices, i.e.,

$$P = D_1 D_2 D_3 \tag{A.2}$$

then, its elements can be written as

$$P_{ik} = \sum_a \sum_b d^1_{ia} d^2_{ab} d^3_{bk} \quad , \tag{A.3}$$

$$P_{il} = \sum_a \sum_b d^1_{ia} d^2_{ab} d^3_{bl} \quad , \tag{A.4}$$

$$P_{jl} = \sum_r \sum_s d^1_{jr}\, d^2_{rs}\, d^3_{sl} , \qquad (A.5)$$

and $$P_{jk} = \sum_r \sum_s d^1_{jr}\, d^2_{rs}\, d^3_{sk} , \qquad (A.6)$$

where a, b, r, s, = 1, 2, 3, 4.

For the case under consideration and using summation rule mentioned in chapter II, eq. (A.1) gives

$$P\Big|^{ij}_{kl} = (d^1_{ia}\, d^2_{ab}\, d^3_{bk})(d^1_{jr}\, d^2_{rs}\, d^3_{sl}) - (d^1_{ia}\, d^2_{ab}\, d^3_{bl})(d^1_{jr}\, d^2_{rs}\, d^3_{sk}). \quad \ldots . \qquad (A.7)$$

Rearranging yields

$$P\Big|^{ij}_{kl} = (d^1_{ia}\, d^1_{sr})(d^2_{ab}\, d^2_{rs})(d^3_{bk}\, d^3_{sl} - d^3_{bl}\, d^3_{sk}) . \qquad (A.8)$$

But, $$d^3\Big|^{bs}_{kl} = d^3_{bk}\, d^3_{sl} - d^3_{bl}\, d^3_{sk} . \qquad (A.9)$$

Thus eq. (A.8) can be written as

$$P\Big|^{ij}_{kl} = (d^1_{ia}\, d^1_{jr})(d^2_{ab}\, d^2_{rs})\, d^3\Big|^{bs}_{kl} . \qquad (A.10)$$

In eq. (A.10) all indices run from 1 to 4.

If one assigns values of a, b, r and s in eq. (A.10), there is a possibility of having terms like $d^1_{ia}\, d^1_{jr}\, (d^2_{as}\, d^2_{rb})\, d^3\Big|^{sb}_{kl}$ in the summation for the assigned values of the indices. Noting that $d^3\Big|^{sb}_{kl} = -d^3\Big|^{bs}_{kl}$ (skew symmetry) and restricting b to be less than s (so that double summation will not occur), it is possible to obtain

$$P\Big|^{ij}_{kl} = (d^1_{ia}\, d^1_{jr})(d^2_{ab}\, d^2_{rs} - d^2_{as}\, d^2_{rb})\, d^3\Big|^{bs}_{kl} , \quad (b < s). \qquad (A.11)$$

But, $d^2_{ab}\, d^2_{rs} - d^2_{as}\, d^2_{rb} = d^2 \begin{vmatrix} ar \\ bs \end{vmatrix}$. (A.12)

Using eq. (A.12) eq. (A.11) reduces to

$$P \begin{vmatrix} ij \\ kl \end{vmatrix} = (d^1_{ia}\, d^1_{jr}) \; d^2 \begin{vmatrix} ar \\ bs \end{vmatrix} \; d^3 \begin{vmatrix} bs \\ kl \end{vmatrix} . \tag{A.13}$$

Using similar argument as before one can readily reduce eq. (A.13)

to $P \begin{vmatrix} ij \\ kl \end{vmatrix} = d^1 \begin{vmatrix} ij \\ ar \end{vmatrix} \; d^2 \begin{vmatrix} ar \\ bs \end{vmatrix} \; d^3 \begin{vmatrix} bs \\ kl \end{vmatrix}$, $(a < r$ and $b < s)$. (A.14)

By analogy to eq. (A.14) the case for $n > 3$ can be written as

$$P \begin{vmatrix} ij \\ kl \end{vmatrix} = d^1 \begin{vmatrix} ij \\ mn \end{vmatrix} \; d^2 \begin{vmatrix} mn \\ op \end{vmatrix} \; . \; . \; . \; d^{n-1} \begin{vmatrix} st \\ uv \end{vmatrix} \; d^n \begin{vmatrix} uv \\ kl \end{vmatrix} . \tag{A.15}$$

THEOREM 2.

Subdeterminants of the G matrices don't contain products of like exponentials.

Proof :-

We know that

$$G_m = T_m \, E_m \, T_m^{-1} . \tag{A.16}$$

Using eq. (A.15) the second order subdeterminants of G_m can be put in the following form.

$$\mathcal{G}^m \begin{vmatrix} ij \\ kl \end{vmatrix} = t^m \begin{vmatrix} ij \\ ab \end{vmatrix} \; \mathcal{e}^m \begin{vmatrix} ab \\ cd \end{vmatrix} \; \tilde{t}^m \begin{vmatrix} cd \\ kl \end{vmatrix} , \quad (a < b, \; c < d), \tag{A.17}$$

where $\mathcal{e}^m \begin{vmatrix} ab \\ cd \end{vmatrix} = \det E_m$ and $\tilde{t}^m \begin{vmatrix} cd \\ kl \end{vmatrix}$ are subdeterminants of T_m^{-1} .

A brief glance at eq. (3.46) is enough to conclude

$$\mathcal{e}^m \begin{vmatrix} ab \\ cd \end{vmatrix} = 0, \qquad (ab \neq cd, \; dc). \tag{A.18}$$

Eq. (A.18) declares that for subdeterminants of E_m not to vanish we must have

$$ab = cd . \tag{A.19}$$

Therefore, eq. (A.17) can be written as

$$g^m \Big|_{kl}^{ij} = t^m \Big|_{ab}^{ij} \quad \tilde{t}^m \Big|_{kl}^{cd} \quad e^m \Big|_{ab}^{ab} , \qquad (a < b). \tag{A.20}$$

One can easily see from eq. (3.46) that $e^m \Big|_{ab}^{ab}$ does not contain products of like exponentials. We also know that T and T^{-1} do not contain exponential terms at all. Therefore, the subdeterminants of G_m matrices also do not contain products of like exponentials.

APPENDIX B

In eq. (3.54) G_m is given by

$$G_m = T_m E_m T_m^{-1} \quad . \tag{B.1}$$

Using eqs. (3.36), (3.46) and (3.39) for T_m, E_m and T_m^{-1} respectively, the algebric expressions for the second order subdeterminants of the G_m matrix can be written as follows:

$$q^m \begin{vmatrix} 12 \\ 12 \end{vmatrix} = q^m \begin{vmatrix} 34 \\ 34 \end{vmatrix} = -2\gamma_m (\gamma_m + 1) + (2\gamma_m^2 + 2\gamma_m + 1)\,\mathrm{CHCK}$$

$$- \left[(\gamma_m + 1)^2 + \gamma_m^2 \tilde{h}_m^2 \tilde{k}_m^2\right] \mathrm{SHSK},$$

$$q^m \begin{vmatrix} 12 \\ 13 \end{vmatrix} = q^m \begin{vmatrix} 24 \\ 34 \end{vmatrix} = (\varrho_m \lambda \zeta)^{-1} (-\mathrm{CHSK} + \tilde{h}^2\,\mathrm{SHCK}),$$

$$q^m \begin{vmatrix} 12 \\ 14 \end{vmatrix} = q^m \begin{vmatrix} 12 \\ 23 \end{vmatrix} = q^m \begin{vmatrix} 14 \\ 34 \end{vmatrix} = q^m \begin{vmatrix} 23 \\ 34 \end{vmatrix} =$$

$$- i\,(\varrho_m \lambda^2 \zeta)^{-1} \left[(2\gamma_m + 1)(1-\mathrm{CHCK}) + (\gamma_m + 1 + \gamma_m \tilde{h}_m^2 \tilde{k}_m^2)\,\mathrm{SHSK}\right] ,$$

$$q^m \begin{vmatrix} 12 \\ 24 \end{vmatrix} = q^m \begin{vmatrix} 13 \\ 34 \end{vmatrix} = (\varrho_m \lambda^2 \zeta)^{-1} (\mathrm{SHCK} - \tilde{k}_m^2\,\mathrm{CHSK}),$$

$$q^m \begin{vmatrix} 12 \\ 34 \end{vmatrix} = -(\varrho_m \lambda^2 \zeta)^{-2} \left[2(1-\mathrm{CHCK}) + (1 + \tilde{h}^2 \tilde{k}_m^2)\,\mathrm{SHSK}\right] ,$$

$$q^m \begin{vmatrix} 13 \\ 12 \end{vmatrix} = q^m \begin{vmatrix} 34 \\ 24 \end{vmatrix} = -(\varrho_m \lambda^2 \zeta)\left[\gamma_m^2 \tilde{k}_m^2\,\mathrm{CHSK} - (\gamma_m + 1)^2\,\mathrm{SHSK}\right] ,$$

$$q^m \begin{vmatrix} 13 \\ 13 \end{vmatrix} = q^m \begin{vmatrix} 24 \\ 24 \end{vmatrix} = \mathrm{CHCK},$$

$$q^m \begin{vmatrix} 13 \\ 14 \end{vmatrix} = q^m \begin{vmatrix} 13 \\ 23 \end{vmatrix} = q^m \begin{vmatrix} 14 \\ 24 \end{vmatrix} = q^m \begin{vmatrix} 23 \\ 24 \end{vmatrix} = i\left[(\gamma_m + 1)\mathrm{SHCK} - \gamma_m^2 \tilde{k}^2 \mathrm{CHSK}\right] ,$$

$$q^m \begin{vmatrix} 13 \\ 24 \end{vmatrix} = -\tilde{k}_m^2\,\mathrm{SHSK}, \tag{B.2}$$

$$g^m\Big|_{12}^{14} = g^m\Big|_{12}^{23} = g^m\Big|_{14}^{34} = g^m\Big|_{23}^{34} = -i(\rho_m \lambda^2 \xi)\Big\{\gamma_m(\gamma_m+1)(2\gamma_m+1)$$
$$\cdot\,(1-CHCK) + (\gamma_m+1)^3 + \Big[\gamma_m^3 \tilde{h}_m^2 \tilde{k}_m^2\Big]\ SHSK\Big\}\ ,$$

$$g^m\Big|_{13}^{14} = g^m\Big|_{13}^{23} = g^m\Big|_{14}^{24} = g^m\Big|_{23}^{24} = -i\left[(\gamma_m+1)\,CHSK - \gamma_m \tilde{h}_m^2\,SHCK\right],$$

$$g^m\Big|_{14}^{14} = g^m\Big|_{23}^{23} = 1 + 2\gamma_m(\gamma_m+1)(1-CHCK) + \left[(\gamma_m+1)^2 + \gamma_m^2 \tilde{h}_m^2 \tilde{k}_m^2\ SHSK\right],$$

$$g^m\Big|_{23}^{14} = g^m\Big|_{14}^{23} = g^m\Big|_{14}^{14} - 1\ ,$$

$$g^m\Big|_{12}^{24} = g^m\Big|_{13}^{34} = -(\rho_m \lambda^2 \xi)\left[(\gamma_m+1)^2\,CHSK - \gamma_m^2 \tilde{h}_m^2\,SHCH\right],$$

$$g^m\Big|_{13}^{24} = -\tilde{h}_m^2 SHSK,$$

$$g^m\Big|_{12}^{34} = -(\rho_m \lambda^2 \xi)\Big\{2\gamma_m^2(\gamma_m+1)^2(1-CHCK)$$
$$+\left[(\gamma_m+1)^4 + \gamma_m^4 \tilde{h}_m^2 \tilde{k}_m^2\right] SHSK\Big\}.$$

where

$$\lambda = s/\xi \qquad \gamma_m = \frac{2\xi^2 \beta_m}{s^2}$$

$$\tilde{h}_m = \xi^{-1}\left(\xi^2 + \frac{s^2}{\alpha_m^2}\right)^{1/2}, \qquad \tilde{k}_m = \xi^{-1}\left(\xi^2 + \frac{s^2}{\beta_m^2}\right)^{1/2}, \tag{B.3}$$

$$SH = \tilde{h}_m^{-1}\sinh(\xi \tilde{h}_m d_m), \qquad SK = \tilde{k}_m^{-1}\sinh(\xi \tilde{k}_m d_m),$$

$$CH = \cosh(\xi \tilde{h}_m d_m) \qquad CK = \cosh(\xi \tilde{k}_m d_m).$$

APPENDIX C

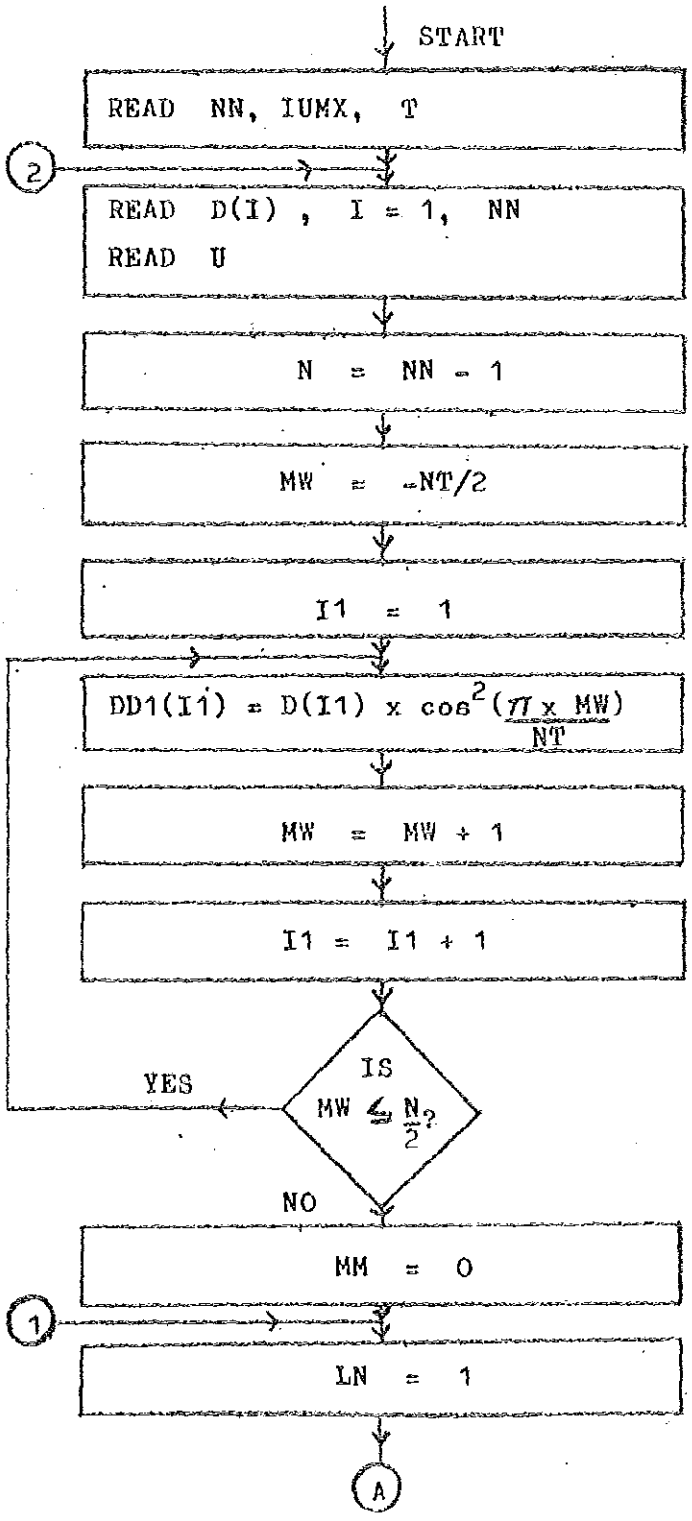
START
READ NN, IUMX, T
2
READ D(I) , I = 1, NN
READ U
N = NN - 1
MW = -NT/2
I1 = 1
DD1(I1) = D(I1) x cos^2($\frac{\pi \times MW}{NT}$)
MW = MW + 1
I1 = I1 + 1
IS
MW ≤ $\frac{N}{2}$?
YES
NO
MM = 0
1
LN = 1
A

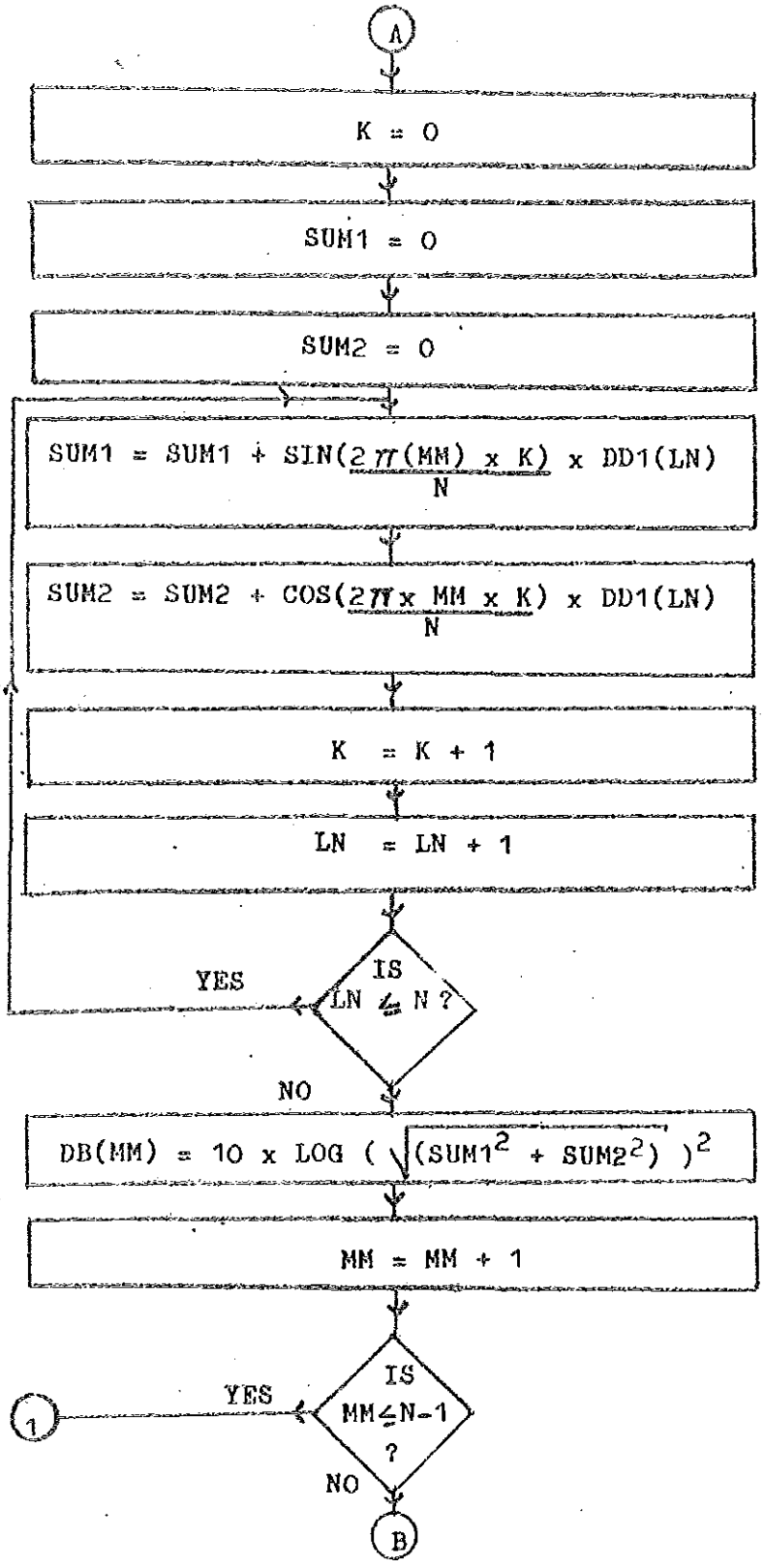
A
K = 0
SUM1 = 0
SUM2 = 0
SUM1 = SUM1 + SIN(2π(MM) x K / N) x DD1(LN)
SUM2 = SUM2 + COS(2π x MM x K / N) x DD1(LN)
K = K + 1
LN = LN + 1
IS LN ≤ N ?
YES
NO
DB(MM) = 10 x LOG (√(SUM1² + SUM2²))²
MM = MM + 1
IS MM ≤ N-1 ?
YES
NO
1
B

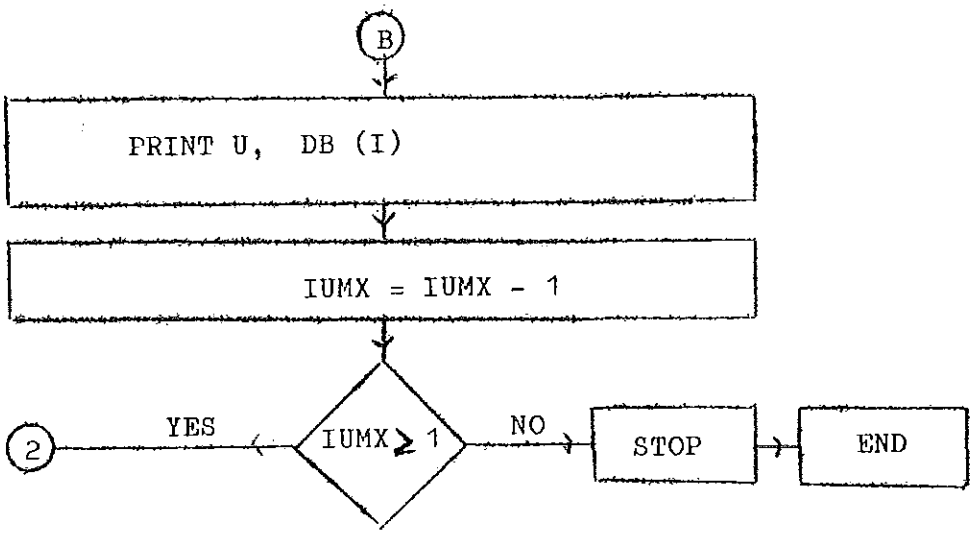

Fig. C1 Computer program flow chart for windowing, evaluating descrete Fourier transform and displaying instantaneous amplitudes in db.

REFERENCES

Achenbach, J.D. (1975). Wave propagation in elastic solids, North-Holland publishing company, Amesterdam.

Aki, K. and P.G. Richards (1980). Quantitative seismology, W.H. Freeman and company, San Fransisco.

Berckhemer, H., B. Baier, H. Bartelsen, A. Behle, H. Burkhardt, H. Gebrande, J. Makris, H. Menzel, H. Miller, and R.Vees (1975). Deep seismic soundings in the Afar region and on the highland of Ethiopia. In Pilger, A. and A. Rosler (edit.), Afar Depression of Ethiopia 1, 89-107.

Brigham, E.O. (1974). The Fast Fourier transform, Prentice-Hall, Inc., New Jersy.

Dunkin, J.W. (1965). Computation of modal solutions in layered elastic media at high frequencies, Bull. Seism. Soc. Am. 55, 335-358.

Gumper, F. and P.W. Pomeroy (1970). Seismic wave velocities and earth structure on the African continent, Bull. Seism. Soc. Am. 60, 651-668.

Haskell, N.A. (1953). The dispersion of surface waves on multi-layered media, Bull. Seism. Soc. Am. 43, 17-34.

Jones, P.B. (1968). Surface-wave dispersion and crustal structure between the Gulf of Aden and Addis Ababa, Bull. Geophys. Obs. 12, 19-26.

Knopoff, L. (1964). A matrix method of Elastic wave problem, Bull. Seism. Soc. Am. 54, 431-438.

Landisman, M., A. Dziervonski, and Y. Sato. (1969). Recent improvements in the analysis of surface wave observations, Geoph. J.R. Astr. Soc. 17, 369-403.

Makris, J., H. Menzel and J. Zimmermann (1972). A preliminary interpretation of the gravity field of Afar, North east Ethiopia, Tectonophysics 15, 1, 31-39.

Makris, J., H. Menzel, J. Zimmermann and P. Gouin (1975). Gravity field and crustal structure of north Ethiopia. In Pilger, A. and A. Rosler (edit.), Afar Depression of Ethiopia 1, 135-144.

Payo, G. (1967). Crustal structure of the mediterranean sea by surface waves. Part I. Group velocity, Bull. Seism. Soc. Am. 57, 151-172.

Pfeffer, R.L. and J. Zarichny (1963). Acoustic - gravity wave propagation in an atmosphere with two sound channels, Geofis. pura appl. 55, 175-199.

Ruegg, J.C. (1975). Main results about the crustal and uppermantle structure of the Djibouti region (T.F.A.I.). In Pilger, A. and A. Rosler (edit.), Afar Depression of Ethiopia 1, 120 -134.

Searle, R.C. and P. Gouin (1971) . An analysis of some local earthquake phases originating near the Afar Triple junction, Bull. Seism. Soc. Am. 61, 1061-1071.

Searle, R.C. (1975). The dispersion of surface waves across southern Afar. In Pilger, A. and A. Rosler (edit.),

Afar Depression of Ethiopia 1, 113-120.

Sokolnikoff, I.S. (1956). Mathematical theory of Elasticity, McGraw-Hill company, Inc., New York.

Talwani, M., G.H. Sutton and J.L. Worzel (1959). Crustal section across the Puerto Rico Trench, J. Geophys. Res. 64, 10, 1545-1555.

Thomson, W.T. (1950). Transmission of elastic waves through a stratified solid medium, J. Appl. Phys. 21, 81-93.

Tryggvason, E. (1962). Crustal structure of the Iceland region from dispersion of surface waves, Bull. Seism. Soc. Am. 52, 359-388.